J. Earth Syst. Sci. (2020)129 73
https://doi.org/10.1007/s12040-019-1332-1

Evidence of Archaean metamorphism from the Yerrabali schist belt of Eastern Dharwar craton from EPMA dating of monazite

Sankha Das[1,*], Sandip Nandy[2], G Ramachandran[3] and Shampa Khan[2]

[1]*National Mission-IA, Geological Survey of India, Kolkata, India.*
[2]*EPMA Laboratory, Geological Survey of India, Kolkata, India.*
[3]*State Unit Telangana, Geological Survey of India, Hyderabad, India.*
**Corresponding author. e-mail: sankhad56@gmail.com*

MS received 2 February 2019; revised 2 October 2019; accepted 5 November 2019

The Dharwar craton is divided in to the Western and Eastern Dharwar craton (WDC and EDC) by the N–S trending Chitradurga Shear zone. The EDC mainly consists of late Archean granites interspersed with N–S trending linear schist belts. The Yerrabali Schst belt (YSB) is located at the north-eastern corner of the EDC, near the Karimnagar granulite belt. The YSB is metamorphosed in middle-upper amphibolite facies and consists of Banded Magnetite Quartzite (BMQ), ferruginous quartzite, ultramafics, quartz–cordierite–gedrite ± garnet bearing quartzite, dolomite, amphibolite, deformed metapyroxenite, tremolite schist, sillimanite–garnet–cordierite schist, and dolerite dykes. We have dated monazites in the sillimanite–garnet–cordierite schist, exposed at the SW part of the YSB by EPMA chemical method. So far no dates are available from the YSB. The monazite chemical ages with three distinct populations, viz., 2658 ± 42, 2817 ± 19 and 3097 ± 34 Ma, probably correspond to three distinct metamorphic phases. The peak metamorphism at around 2800 Ma corresponds with the garnet and cordierite growth. A temperature of 673°C and a pressure of 4.7 kb have been estimated for peak metamorphism.

Keywords. Yerrabali schist belt; monazite dating; Eastern Dharwar craton; EPMA chemical dating.

1. Introduction

Monazite is a phospahate mineral (LREE, ThO_2) PO_4 which preferentially incorporates LREE (mainly La, Ce and Nd). It crystallizes in orthorhombic system and consists of a distorted nine oxygen coordinated polyhedron and PO_4 tetrahedra (Williams *et al.* 2007). Monazite occurs in many igneous and metamorphic rocks. As it contains high Th and U (Th values are much higher than U) and very low amount of non-radiogenic Pb, it is being used for Th–U–Pb dating (Williams and Jercinovic 2002). The diffusion of major and trace elements is also very slow through monazite, which helps in retaining older ages through younger metamorphic events (Williams and Jercinovic 2002). The Dharwar craton is divided in to two parts viz. the Western Dharwar craton (WDC) and the Eastern Dharwar craton (EDC). The EDC is separated from the WDC by N–S trending steep sinistral Chitradurga shear zone (Chadwick *et al.* 2000). The EDC consists of late Archean calc-alkaline granitoids with several N–S trending narrow schist belts (Chadwick *et al.* 2000; Jayananda *et al.* 2000). The northeastern boundary of EDC is separated from the Bastar

Published online: 15 February 2020

craton by Permo-Carboniferous sediments of the Godavari graben (Prakash *et al.* 2017). Maibam *et al.* (2011) dated detrital zircons from the meta-sediments in the southwestern part of the EDC to be >3.0 Ga old with a few dates going up to 3.4 Ga. Maibam *et al.* (2016) dated zircons from a quartzite near Sarkasanahalli village (located at the southern part of EDC) at >3.0 Ga. Adhikary *et al.* (2016) dated magmatic zircon at 3526 ± 96 Ma from TTG gneisses around the Khammam schist belt located at the northeastern part of the EDC and considered it as the oldest crustal component of EDC. This suggests that the protolithic ages of meta-sediments of EDC can be as old as 3.5 Ga. In this paper, we concentrate on bringing out the metamorphic age of the YSB situated in the northeastern part of the EDC by U–Th–Pb (total) dating of monazite with EPMA along with the estimate of the pressure–temperature conditions of metamorphism.

2. Regional geology

The YSB is situated towards the northeastern margin of the EDC in the Karimnagar district of the Telangana state in the Survey of India toposheet No. 56N/08, bounded by lattitudes 18°0′00″–18°03′30″N and longitudes 79°22′00″–79°25′00″E (figure 1a). YSB is a NW–SE trending 10 km long and 4 km wide belt occurring around 100 km south of the Karimnagar granulite belt (figure 1b). Rajesham and Nagarajan (1990) carried out systematic geological mapping in parts of the Karimnagar and Nalgonda districts and identified NW–SE trending 150 km long and 20 km wide Karimnagar granulite belt (KGB) along the southern flank of the Godavari graben, which separates the Dharwar craton and the Bastar craton. It is suggested that the KGB is the remnant of an Archean supracrustal–granite association which has undergone granulite facies metamorphism at ∼2.5 Ga. This ancient orogenic belt has been exhumed during the early Proterozoic time (Santosh *et al.* 2003). The Bhopalpatnam granulite belt occurs to the east of KGB. So far no geochronological data are available from the YSB.

The YSB is surrounded by granitoids of the EDC. Gupta *et al.* (GSI unpublished report F.S.2014–15) reported two types of granites, viz., monzogranite and granodiorite and suggested that they have intruded the schist belt. The main rock types exposed in YSB are Banded Magnetite Quartzite (BMQ), ultramafics, quartz–cordierite–gedrite ± garnet bearing quartzite, sillimanite–garnet–cordierite schist, meta-dolomite, amphibolite, ferruginous quartzite, deformed garnet bearing granite, meta-pyroxenite, tremolite schist, foliated quartzite, quartz vein and dolerite dyke. The area is highly deformed. Mainly three sets of deformation are found in the lithounits of Yerrabali schist belt. The first stage of deformation is represented by isoclinal F1 folds and the second stage by tight to isoclinal F2 folds. At places, the F1 and the F2 folds show hook shaped type-3 interference patterns. The plunge of the F2 folds varies from shallow to moderate either towards NW or towards SE. F2 folds control the shape and structure of the YSB, which shows a broad synformal structure plunging moderately towards south. The third set of deformation is defined by folds with nearly E–W trending vertical axial plane and axis.

During our work, several monazites were found in sillimanite–garnet–cordierite schist, exposed at the SW part of the Yerrabali schist belt. The rock essentially consists of sillimanite, garnet, quartz, cordierite, K-feldspar and biotite. Monazite grains in sillimanite–garnet–cordierite schist occur in matrix and also as inclusions within garnet, cordierite and biotite grains. Total 27 monazite grains were analyzed containing 90 spot analyses. La and Ce followed by oxides of Gd, Nd and Pr are the most abundant of REE in monazite. The elemental value of U, Pb and Th ranges from 0.082–0.681%, 0.436–1.699% and 2.803–9.307%, respectively.

3. Analytical methods

The monazite analysis was carried out on CAMECA SX 100 with five WDS spectrometers at EPMA Laboratory, Gelological Survey of India, Kolkata. The standard error on the analyses is of the order of 2–3% for monazites with 1500–2000 ppm total Pb. The analytical conditions are: accelerating voltage of 20 KV, beam current of 200 nA and beam size of 1 micron. The crystals selected for this analysis are PET in Spectrometer 1 (SP1), TAP in Spectrometer 2 (SP2), LPET in Spectrometer 3 (SP3), LIF in Spectrometer 4 (SP4) and PET in Spectrometer 5 (SP5). The X-ray lines selected were Kα for Ca, Si, P; Lα for La, Ce, Y, Nd, Sm, Gd, Dy and Lβ for Pr; *M*α for Th and *M*β for Pb and U. Natural standards are used for calibration of Si, Ca, P; whereas all the REE standards

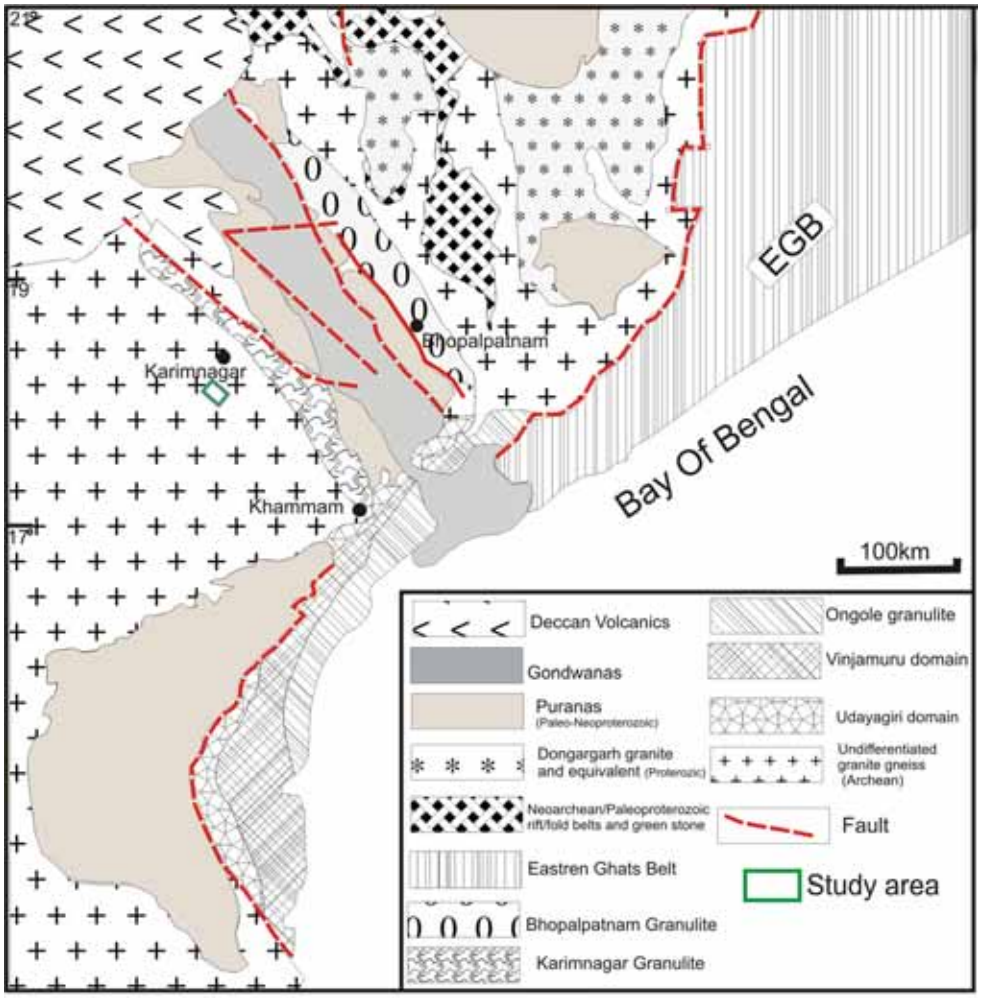

Map modified after Saha and Patranabis-Deb, 2013

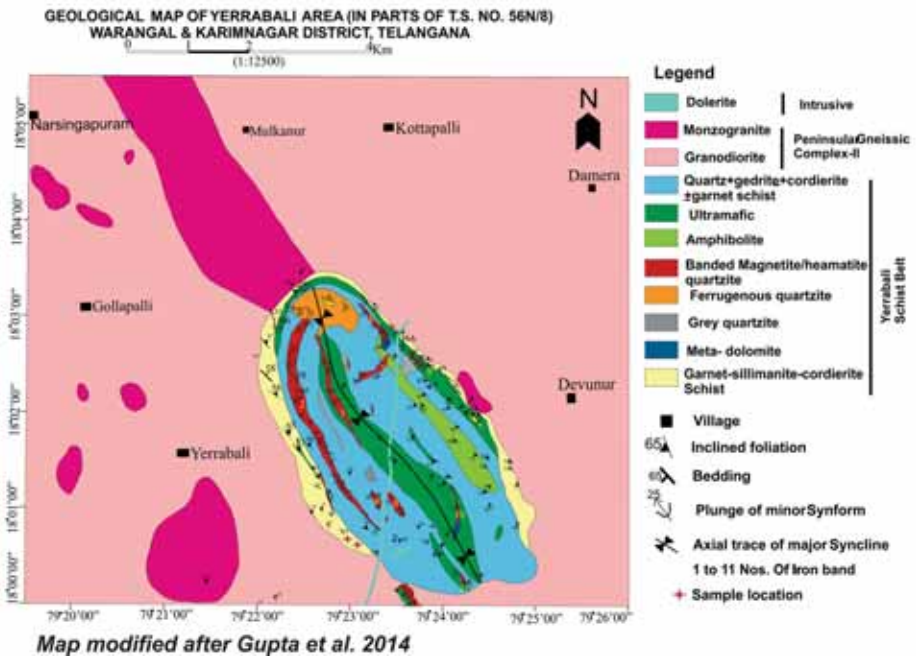

Map modified after Gupta et al. 2014

Figure 1. Generalised geological map of (**a**) generalised geological map showing Part of Eastern Dharwar Craton, Bastar Craton Eastern Ghat Belt and Deccan volcanics and (**b**) Yerrabali schist belt modified after Gupta and Nandhagopal (2014).

are in glass. U, Pb and Th are calibrated from natural uraninite, galena and thorite, respectively. Matrix correction by PAP (Pouchou and Pichoir) is used. Corrections are applied for the following interferences Pb*M*α–Th*Mz*, PbMα–Y*Lc2* and U*M*β–ThM3N4.

4. Metamorphism

Cordierite is indicative of low P metamorphism (Bucher and Frey 1994; Winter 2001) and generally forms in contact metamorphism, but cordierite is also reported from regionally metamorphosed metapelites (Nathan *et al.* 1995; Perera 1984). Coupled occurrence of garnet and cordierite is reported from the high grade metapelites of Srilanka (Perera 1984) and has been interpreted to have formed at 5.5–6 kb pressure and 700°C tempertature. Nathan *et al.* (1995) reported the occurrence of garnet (almandine)–cordierite–biotite–sillimanite–K-feldspar bearing assemblages from Tamil Nadu and suggested that the assemblage formed under regional metamorphism (4–6 kb pressure and 700°C temperatures) with an overprint of later thermal metamorphism due to granitic intrusions.

Under amphibolite facies, monazite is associated with the formation of staurolite by break down of garnet (Fitzsimons *et al.* 2005) via the reaction Grt + Chl + Ms = St + Bt + Qtz + H_2O- (1). In the KFMASH system garnet first appears in pelites at nearly 450°C and garnet + biotite becomes stable at near 520°C (Bucher and Frey 1994). Fe-rich biotite breaks down to garnet + K-feldspar at around 600°C through the reaction muscovite + Annite + 3qtz = 1alm + 2Kfs + H_2O and K-feldspar + garnet + biotite can form a stable assemblage above 600°C (Bucher and Frey 1994). In KFMASH system cordierite first becomes stable at a temperature of 530°C (Bucher and Frey 1994). Cordierite + garnet + K-feldspar + biotite ± sillimanite is a characteristic assemblage of high grade gneisses at a temperature of 700 ± 50°C (Bucher and Frey 1994). Garnet–cordierite–sillimanite–quartz bearing assemblages were reported from the Archaean Bundelkhand craton by Singh and Dwivedi (2009). They deduced maximum temperature of 730°C and pressure of 5.4 kb from core compositions of porphyroblast and 640°C and 5.1 kb from the rim composition of pophyroblasts and interpreted granulite grade metamorphism.

In the present case, the metapelite contains garnet, biotite, sillimanite/fibrolite, K-feldspar (both perthite and microclene) and cordierite as major phases and magnetite, ilmenite as accessory mineral. Under microscope, the rock shows development of S_1 schistosity defined by oriented biotite and sillimanite/fibrolite. The schistosity swerves around the K-feldspar (perthite) prophyroblast (figure 2a). The sillimanite grains are needle shaped, contain cross-fracture perpendicular to the grain boundary. Sillimanite/fibrolite grains are of two types, one is aligned with the S_1 schistosity and other (fibrolite) is oriented at a high angle to the S_1 schistosity (figure 2b), probably formed after D_1 deformation. Garnet, cordierite and K-feldspar formed earlier than D_1 deformation, as evident from the schistosity swerving around K-feldspar, cordierite and garnet porphyroblasts (figure 2c). K-feldspar and cordierite contain inclusion of biotite ± quartz ± sillimanite (figure 2d, e), while garnet contains inclusions of biotite and quartz. This suggests that cordierite, garnet and K-feldspar might have formed by the reaction Bt + Sil + Qtz = Crd + Grt + Kfs + H_2O (Bucher and Frey 1994). Later formed fibrolite and coarse lath shaped biotite cross-cuts the schistosity and also cross-cut the grain boundary of K-feldsapar and cordierite prophyroblasts (figure 2f). EPMA analyses show that in garnet, almandine component ranges from 83–86%. The X_{Mg} of biotite varies from 0.38 to 0.43 and that of cordierite ranges from 0.57 to 0.60. The Ti content of biotite ranges from 0.3 to 0.57 atom per formula unit (apfu on 24 oxygen basis). Garnet biotite thermometry (after Holdaway 2000) from the present samples show temperature range of 544–630°C. Garnet–cordierite thermometry (after Dwivedi *et al.* 1998) show temperature range from 616 to 673°C. Garnet cordierite barometry (after Dwivedi *et al.* 1997) show pressure range of 3–4.7 kb and garnet–biotite–Al_2SiO_5–quartz (GBAQ) barometry after Wu (2017) show pressure range from 2.8 to 4.3 kb.

5. Monazite chemistry and geochronology

Monazite analysis by both ICPMS and by EPMA is being used for dating of igneous and metamorphic rocks. In EPMA dating Th, U and total Pb of monazite is measured and all of the Pb is considered as radiogenic. Pb diffusion in monazite is extremely slow and isotopic closure temperature of

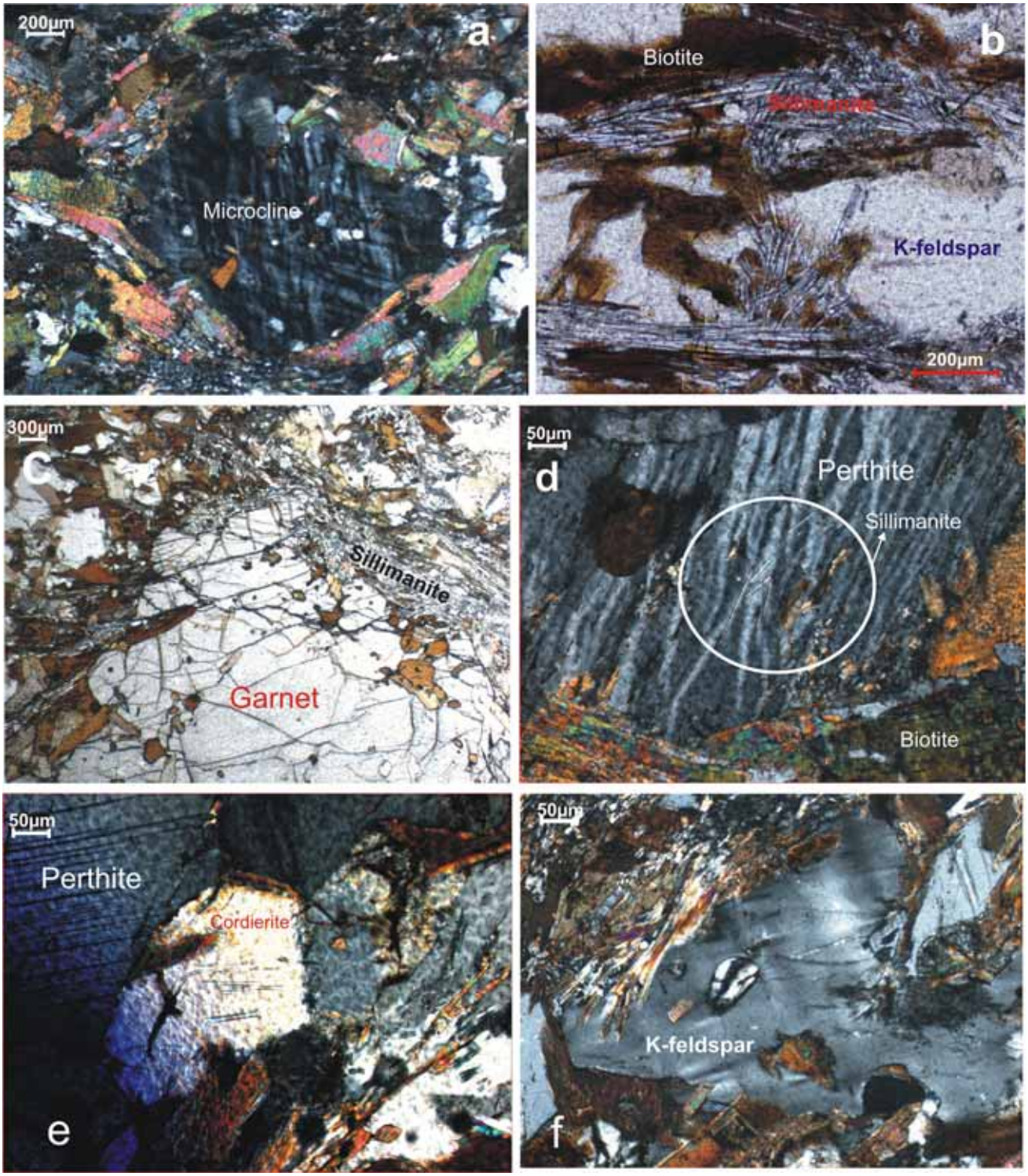

Figure 2. Photomicrograph of (**a**) K-feldspar porphyroblast, (**b**) two types of sillimanite, one is aligned with the schistosity and the other is oriented at a high angle to the schistosity, (**c**) shistosity defined by sillimanite swerving around garnet porphyroblast. The garnet is fractured and contains inclusions of biotite, (**d**) K-feldspar containing inclusion of sillimanite, (**e**) cordierite containing inclusion of sillimanite, and (**f**) sillimanite intruding the boundary of a K-feldspar grain.

Pb is around 800°C (Williams *et al.* 2007; Hoisch *et al.* 2008). For Pb diffusion to be of any significance, a monazite grain has to spend considerable time at or above 800°C (Williams *et al.* 2007). Initial monazite ages are calculated by iteratively solving the Montel *et al.* (1996) equation. Age error

Table 1a. *EPMA analysis of monazite grains.*

Sl. no.	Si	P	Ca	Y	La	Ce	Pr	Nd	Sm	Gd	Dy	U	Th	Pb	U (1σ)	Th (1σ)	Pb (1σ)
a																	
1	0.014	1.012	0.077	0.017	0.207	0.354	0.046	0.124	0.024	0.039	0.006	0.477	6.503	1.235	0.004	0.010	0.030
2.	0.018	1.009	0.066	0.013	0.220	0.370	0.045	0.124	0.023	0.039	0.004	0.359	5.554	1.058	0.003	0.008	0.027
3.	0.012	1.016	0.066	0.013	0.216	0.372	0.047	0.125	0.024	0.037	0.005	0.354	5.290	1.003	0.003	0.008	0.026
4.	0.017	1.013	0.076	0.017	0.207	0.356	0.044	0.121	0.024	0.038	0.006	0.454	6.424	1.244	0.004	0.009	0.030
5.	0.015	1.012	0.076	0.018	0.208	0.357	0.045	0.121	0.024	0.039	0.006	0.459	6.354	1.235	0.004	0.009	0.030
6.	0.014	1.014	0.076	0.019	0.207	0.357	0.045	0.119	0.024	0.040	0.006	0.463	6.363	1.235	0.004	0.009	0.030
7.	0.013	1.022	0.064	0.015	0.219	0.367	0.044	0.119	0.023	0.038	0.005	0.395	5.290	1.040	0.004	0.008	0.027
8.	0.013	1.023	0.032	0.052	0.221	0.375	0.046	0.120	0.024	0.038	0.010	0.145	3.173	0.538	0.003	0.005	0.018
9.	0.039	0.993	0.086	0.034	0.200	0.342	0.043	0.114	0.019	0.032	0.006	0.336	7.936	1.290	0.003	0.012	0.031
10.	0.021	1.004	0.087	0.009	0.213	0.359	0.043	0.116	0.019	0.030	0.003	0.282	8.234	1.309	0.003	0.012	0.032
11.	0.031	0.989	0.076	0.009	0.212	0.366	0.046	0.124	0.020	0.030	0.004	0.245	8.226	1.253	0.003	0.012	0.031
12.	0.026	0.995	0.081	0.000	0.223	0.371	0.044	0.120	0.017	0.028	0.002	0.218	8.287	1.235	0.003	0.012	0.031
13.	0.026	0.996	0.083	0.000	0.219	0.368	0.045	0.120	0.018	0.028	0.002	0.236	8.278	1.235	0.003	0.012	0.031
14.	0.040	0.982	0.075	0.000	0.223	0.375	0.045	0.121	0.017	0.028	0.002	0.250	8.226	1.263	0.003	0.012	0.031
15.	0.033	0.981	0.079	0.000	0.223	0.373	0.046	0.123	0.018	0.029	0.002	0.195	8.489	1.253	0.003	0.012	0.031
16.	0.033	0.991	0.078	0.004	0.219	0.367	0.046	0.119	0.017	0.028	0.002	0.268	8.305	1.290	0.003	0.012	0.032
17.	0.023	1.014	0.080	0.025	0.203	0.344	0.043	0.113	0.018	0.031	0.006	0.313	8.024	1.244	0.003	0.011	0.030
18.	0.028	1.002	0.075	0.000	0.221	0.367	0.045	0.119	0.017	0.027	0.002	0.195	8.270	1.179	0.003	0.012	0.029
19.	0.028	0.996	0.075	0.000	0.224	0.373	0.045	0.123	0.016	0.024	0.001	0.173	8.252	1.151	0.003	0.012	0.029
20.	0.030	0.994	0.076	0.000	0.222	0.372	0.045	0.121	0.015	0.025	0.001	0.168	8.481	1.188	0.003	0.012	0.029
21.	0.043	0.979	0.078	0.001	0.221	0.375	0.046	0.121	0.018	0.027	0.002	0.168	8.234	1.114	0.003	0.012	0.028
22.	0.026	0.994	0.078	0.000	0.224	0.373	0.045	0.122	0.016	0.026	0.002	0.168	8.278	1.151	0.003	0.012	0.029
23.	0.031	0.992	0.077	0.000	0.223	0.374	0.045	0.121	0.015	0.024	0.001	0.177	8.568	1.179	0.003	0.012	0.029
24.	0.015	0.397	0.077	0.000	0.149	0.251	0.030	0.081	0.015	0.016	0.001	0.227	8.762	1.198	0.003	0.012	0.029
25.	0.015	1.010	0.069	0.031	0.214	0.358	0.046	0.119	0.020	0.035	0.007	0.286	6.521	1.068	0.003	0.010	0.027
26.	0.011	1.013	0.054	0.039	0.224	0.374	0.046	0.120	0.021	0.037	0.009	0.300	4.245	0.780	0.003	0.006	0.022
27.	0.012	1.012	0.058	0.034	0.220	0.371	0.046	0.120	0.021	0.037	0.007	0.322	5.132	0.891	0.003	0.008	0.024
28.	0.022	1.001	0.086	0.013	0.209	0.352	0.044	0.119	0.020	0.033	0.004	0.318	8.410	1.253	0.003	0.012	0.031
29.	0.009	1.015	0.043	0.043	0.224	0.380	0.047	0.122	0.022	0.038	0.009	0.404	3.111	0.761	0.004	0.005	0.022
30.	0.008	1.013	0.041	0.042	0.226	0.384	0.047	0.124	0.022	0.039	0.009	0.372	2.970	0.696	0.004	0.005	0.021
31.	0.013	1.013	0.050	0.043	0.222	0.370	0.046	0.121	0.021	0.038	0.008	0.322	3.999	0.771	0.003	0.006	0.022
32.	0.011	1.008	0.053	0.040	0.225	0.373	0.046	0.121	0.021	0.038	0.009	0.273	4.385	0.780	0.003	0.007	0.023
33.	0.027	0.996	0.085	0.006	0.215	0.358	0.045	0.119	0.019	0.031	0.003	0.277	8.173	1.207	0.003	0.012	0.030

Table 1a. *(Continued.)*

Sl. no.	Si	P	Ca	Y	La	Ce	Pr	Nd	Sm	Gd	Dy	U	Th	Pb	U (1σ)	Th (1σ)	Pb (1σ)
34.	0.030	0.986	0.082	0.000	0.222	0.369	0.046	0.124	0.017	0.028	0.001	0.186	8.516	1.216	0.003	0.012	0.030
35.	0.030	0.978	0.081	0.000	0.227	0.375	0.048	0.126	0.017	0.028	0.002	0.168	8.252	1.198	0.003	0.012	0.030
36.	0.067	0.966	0.074	0.000	0.223	0.369	0.045	0.121	0.017	0.029	0.002	0.177	7.874	1.133	0.003	0.011	0.029
37.	0.017	1.009	0.078	0.029	0.208	0.348	0.043	0.117	0.019	0.033	0.006	0.336	7.250	1.170	0.003	0.011	0.029
38.	0.023	1.006	0.090	0.026	0.203	0.342	0.042	0.108	0.019	0.031	0.007	0.322	8.103	1.244	0.003	0.012	0.030
39.	0.015	1.014	0.074	0.041	0.206	0.348	0.043	0.112	0.020	0.033	0.007	0.336	6.740	1.123	0.003	0.010	0.029
40.	0.026	1.011	0.073	0.046	0.202	0.339	0.041	0.110	0.019	0.034	0.009	0.363	6.574	1.123	0.003	0.010	0.028
41.	0.011	1.020	0.056	0.043	0.216	0.363	0.043	0.114	0.020	0.036	0.009	0.359	4.790	0.900	0.003	0.007	0.024
42.	0.015	1.014	0.063	0.008	0.222	0.376	0.046	0.120	0.022	0.034	0.005	0.322	5.703	0.993	0.003	0.008	0.026
43.	0.013	1.015	0.062	0.009	0.222	0.377	0.046	0.121	0.021	0.034	0.004	0.309	5.580	0.984	0.003	0.008	0.026
44.	0.024	1.006	0.080	0.000	0.216	0.363	0.044	0.116	0.017	0.027	0.002	0.245	8.322	1.198	0.003	0.012	0.030
45.	0.029	0.997	0.071	0.000	0.224	0.375	0.046	0.119	0.015	0.026	0.001	0.168	7.971	1.086	0.003	0.012	0.028
46.	0.014	1.017	0.073	0.046	0.201	0.341	0.043	0.112	0.020	0.036	0.009	0.345	6.538	1.133	0.003	0.010	0.028
47.	0.018	1.010	0.075	0.023	0.207	0.355	0.044	0.117	0.019	0.033	0.007	0.291	7.189	1.123	0.003	0.010	0.028
48.	0.020	0.997	0.084	0.000	0.222	0.364	0.046	0.119	0.019	0.031	0.002	0.318	8.006	1.207	0.003	0.012	0.030
49.	0.027	0.993	0.077	0.000	0.224	0.372	0.047	0.121	0.016	0.027	0.001	0.182	8.270	1.123	0.003	0.012	0.029
50.	0.020	1.002	0.080	0.000	0.227	0.367	0.045	0.115	0.018	0.030	0.002	0.259	7.971	1.179	0.003	0.012	0.029
51.	0.019	1.003	0.080	0.000	0.224	0.365	0.045	0.117	0.018	0.030	0.002	0.259	8.076	1.198	0.003	0.012	0.030
52.	0.020	1.001	0.080	0.000	0.224	0.367	0.046	0.117	0.018	0.031	0.002	0.263	7.927	1.179	0.003	0.011	0.029
53.	0.021	1.004	0.079	0.000	0.222	0.365	0.045	0.116	0.018	0.030	0.002	0.263	8.041	1.207	0.003	0.012	0.030
54.	0.022	1.001	0.082	0.000	0.218	0.362	0.044	0.118	0.018	0.030	0.002	0.277	8.401	1.263	0.003	0.012	0.031
55.	0.015	1.010	0.077	0.050	0.200	0.339	0.042	0.113	0.020	0.035	0.010	0.350	7.057	1.198	0.003	0.010	0.029
56.	0.027	0.997	0.077	0.000	0.217	0.365	0.045	0.120	0.018	0.031	0.002	0.218	8.481	1.198	0.003	0.012	0.030
57.	0.027	0.998	0.078	0.000	0.215	0.363	0.046	0.120	0.018	0.032	0.002	0.223	8.516	1.216	0.003	0.012	0.030
58.	0.027	0.998	0.079	0.000	0.217	0.362	0.045	0.119	0.018	0.031	0.002	0.223	8.577	1.244	0.003	0.012	0.031
59.	0.025	1.001	0.077	0.000	0.221	0.365	0.045	0.118	0.017	0.029	0.001	0.223	8.217	1.216	0.003	0.012	0.030
60.	0.026	0.989	0.079	0.000	0.221	0.371	0.047	0.123	0.018	0.032	0.002	0.209	8.032	1.235	0.003	0.012	0.031
61.	0.013	1.005	0.062	0.041	0.214	0.367	0.046	0.121	0.021	0.037	0.008	0.327	5.159	0.984	0.003	0.008	0.026
62.	0.025	0.992	0.078	0.000	0.222	0.370	0.047	0.123	0.018	0.031	0.002	0.218	8.094	1.160	0.003	0.012	0.029
63.	0.022	1.004	0.080	0.003	0.214	0.358	0.046	0.119	0.020	0.032	0.002	0.282	8.182	1.216	0.003	0.012	0.030
64.	0.023	1.005	0.071	0.009	0.214	0.361	0.046	0.120	0.019	0.033	0.003	0.245	7.663	1.160	0.003	0.011	0.029
65.	0.022	1.005	0.078	0.000	0.218	0.361	0.045	0.118	0.018	0.031	0.002	0.259	8.322	1.179	0.003	0.012	0.029
66.	0.014	1.009	0.071	0.030	0.212	0.356	0.044	0.118	0.020	0.035	0.006	0.295	6.864	1.105	0.003	0.010	0.028
67.	0.020	0.996	0.087	0.012	0.215	0.351	0.046	0.116	0.020	0.035	0.005	0.372	8.067	1.337	0.003	0.012	0.032

Table 1a. *(Continued.)*

Sl. no.	Si	P	Ca	Y	La	Ce	Pr	Nd	Sm	Gd	Dy	U	Th	Pb	U (1σ)	Th (1σ)	Pb (1σ)
68.	0.039	0.990	0.088	0.010	0.210	0.349	0.044	0.115	0.019	0.035	0.005	0.354	8.024	1.300	0.003	0.009	0.030
69.	0.028	0.972	0.079	0.014	0.226	0.378	0.050	0.128	0.021	0.037	0.005	0.350	7.918	1.225	0.003	0.012	0.030
70.	0.018	0.998	0.084	0.014	0.213	0.354	0.045	0.118	0.020	0.036	0.005	0.327	8.524	1.374	0.003	0.012	0.033
71.	0.016	0.999	0.095	0.000	0.214	0.354	0.046	0.119	0.021	0.033	0.003	0.304	9.192	1.402	0.003	0.013	0.034
72.	0.018	0.991	0.099	0.000	0.213	0.354	0.046	0.121	0.020	0.033	0.002	0.295	9.219	1.383	0.003	0.013	0.033
73.	0.018	0.992	0.099	0.000	0.214	0.354	0.045	0.120	0.020	0.033	0.002	0.295	9.245	1.383	0.003	0.013	0.033
74.	0.020	0.994	0.100	0.000	0.213	0.350	0.044	0.119	0.020	0.032	0.002	0.295	9.307	1.374	0.003	0.013	0.033
75.	0.020	0.989	0.100	0.000	0.212	0.358	0.045	0.123	0.021	0.033	0.002	0.286	8.762	1.318	0.003	0.013	0.032
76.	0.017	0.959	0.093	0.000	0.214	0.354	0.045	0.120	0.020	0.033	0.003	0.327	8.533	1.355	0.003	0.012	0.032
77.	0.019	0.993	0.096	0.001	0.214	0.356	0.046	0.122	0.021	0.034	0.003	0.268	8.700	1.318	0.003	0.013	0.032
78.	0.019	0.997	0.095	0.000	0.217	0.356	0.045	0.119	0.019	0.032	0.002	0.209	7.980	1.179	0.003	0.012	0.030
79.	0.016	0.978	0.114	0.001	0.214	0.346	0.044	0.113	0.020	0.037	0.003	0.645	8.612	1.643	0.005	0.012	0.037
80.	0.014	0.986	0.110	0.001	0.214	0.351	0.044	0.116	0.020	0.036	0.003	0.550	8.199	1.495	0.004	0.012	0.035
81.	0.013	0.992	0.103	0.002	0.210	0.353	0.045	0.121	0.023	0.036	0.004	0.650	8.533	1.652	0.005	0.012	0.038
82.	0.014	0.993	0.109	0.003	0.211	0.346	0.044	0.114	0.021	0.035	0.003	0.681	8.595	1.699	0.005	0.012	0.038
83.	0.019	0.987	0.120	0.001	0.207	0.338	0.043	0.110	0.020	0.035	0.002	0.259	7.400	1.142	0.003	0.011	0.029
84.	0.066	0.972	0.080	0.000	0.219	0.366	0.045	0.122	0.018	0.029	0.001	0.082	3.260	0.501	0.002	0.005	0.018
85.	0.014	0.988	0.031	0.000	0.252	0.429	0.054	0.148	0.021	0.034	0.001	0.164	4.174	0.687	0.003	0.006	0.021
86.	0.015	0.988	0.043	0.000	0.244	0.414	0.054	0.147	0.021	0.033	0.001	0.091	2.803	0.436	0.002	0.005	0.017
87.	0.013	0.988	0.028	0.000	0.251	0.433	0.057	0.153	0.022	0.034	0.001	0.082	3.999	0.557	0.002	0.006	0.019
88.	0.028	0.984	0.038	0.000	0.243	0.416	0.053	0.145	0.021	0.034	0.001	0.123	9.157	1.235	0.003	0.013	0.031
89.	0.040	0.967	0.073	0.000	0.222	0.374	0.049	0.132	0.018	0.028	0.001	0.259	9.034	1.495	0.003	0.013	0.035
90	0.958	0.095	0.017	0.212	0.354	0.045	0.121	0.020	0.035	0.005	0.095	0.313	9.280	1.485	0.003	0.013	0.035

Table 1b. *Calculated ages of monazite grains.*

Sl. no.	point	Mode of occurence	EXPLICIT AGE (Ma)	AGE error(1σ, Ma)	Age (Ma) Calculated from Montel equation	Age error (Ma,2σ) claculated by Vlach (2010) method	Y
b (# SG= Same Grain)							
1	2 / 1	Matrix	3011	73	3009	123	0.017
2	3 / 1	Matrix	3096	88	3093	133	0.013
3	7 / 1	Matrix (SG)	3061	84	3059	133	0.013
4	7 / 2	Matrix (SG)	3083	75	3081	124	0.017
5	7 / 3	Matrix (SG)	3079	74	3078	124	0.018
6	7 / 4	Matrix (SG)	3070	74	3069	123	0.019
7	7 / 5	Matrix (SG)	3087	80	3085	131	0.015
8	9 / 1	Inclusion within cordierite	2967	98	2966	173	0.052
9	10 / 1	Matrix (SG)	2890	68	2889	122	0.034
10	10 / 2	Matrix (SG)	2908	68	2907	124	0.009
11	10 / 3	Matrix (SG)	2842	67	2841	124	0.009
12	10 / 4	Matrix (SG)	2819	67	2818	125	0.000
13	10 / 5	Matrix (SG)	2800	67	2799	124	0.000
14	10 / 6	Matrix (SG)	2855	68	2854	125	0.000
15	11 / 1	Matrix	2827	67	2826	125	0.000
16	12 / 1	Matrix	2868	68	2867	124	0.004
17	13 / 1	Matrix	2801	65	2799	118	0.025
18	13 / 2	Matrix	2734	65	2733	121	0.000
19	13 / 3	Matrix	2706	65	2705	122	0.000
20	13 / 4	Matrix	2727	65	2726	122	0.000
21	13 / 5	Matrix	2636	64	2635	121	0.001
22	13 / 6	Matrix	2704	65	2703	122	0.000
23	13 / 7	Matrix	2675	63	2674	119	0.000
24	13 / 8	Matrix	2611	62	2610	115	0.000
25	14 / 1	Within biotite (same grain)	2893	72	2892	128	0.031
26	14 / 2	Within biotite (same grain)	2951	84	2950	141	0.039
27	14 / 3	Within biotite (same grain)	2877	90	2875	133	0.034
28	14 / 4	Within biotite (same grain)	2715	65	2714	118	0.013
29	15 / 1	Within biotite (same grain)	3211	95	3209	142	0.043

Table 1b. *(Continued.)*

Sl. no.	point	Mode of occurence	EXPLICIT AGE (Ma)	AGE error(1σ, Ma)	Age (Ma) Calculated from Montel equation	Age error (Ma,2σ) claculated by Vlach (2010) method	Y
30	15 / 2	Within biotite (same grain)	3137	97	3136	148	0.042
31	15 / 3	Within biotite (same grain)	2989	87	2987	144	0.043
32	15 / 4	Within biotite (same grain)	2942	101	2939	144	0.040
33	15 / 5	Within biotite (same grain)	2727	66	2726	122	0.006
34	16 / 3	Within biotite (same grain)	2755	66	2754	124	0.000
35	16 / 4	Within biotite (same grain)	2810	68	2809	127	0.000
36	16 / 5	Within biotite (same grain)	2767	68	2766	127	0.000
37	17 / 1	Inclusion within garnet	2835	69	2833	123	0.029
38	18 / 1	Inclusion within garnet	2770	66	2769	119	0.026
39	19 / 1	Inclusion within garnet (SG)	2884	72	2883	126	0.041
40	19 / 2	Inclusion within garnet (SG)	2900	74	2899	124	0.046
41	19 / 3	Inclusion within garnet (SG)	2974	80	2972	134	0.043
42	19 / 4	Inclusion within garnet (SG)	2937	81	2935	132	0.008
43	19 / 5	Inclusion within garnet (SG)	2979	81	2977	135	0.009
44	20 / 1	Inclusion within garnet (SG)	2703	65	2702	120	0.000
45	20 / 2	Inclusion within garnet (SG)	2647	66	2646	124	0.000
46	20 / 3	Inclusion within garnet (SG)	2956	72	2954	125	0.046
47	20 / 4	Inclusion within garnet (SG)	2808	69	2806	124	0.023
48	21 / 1	Inclusion within garnet (SG)	2726	66	2725	119	0.000
49	21 / 2	Inclusion within garnet (SG)	2632	64	2631	121	0.000
50	22 / 1	Inclusion within cordierite (SG)	2744	66	2742	122	0.000
51	22 / 2	Inclusion within cordierite (SG)	2753	66	2752	122	0.000
52	22 / 3	Inclusion within cordierite (SG)	2750	67	2749	122	0.000
53	22 / 4	Inclusion within cordierite (SG)	2777	67	2776	122	0.000
54	22 / 5	Inclusion within cordierite (SG)	2778	66	2777	121	0.000
55	22 / 6	Inclusion within cordierite (SG)	2933	70	2931	123	0.050
56	22 / 7	Inclusion within cordierite (SG)	2692	65	2691	121	0.000
57	22 / 8	Inclusion within cordierite (SG)	2715	65	2714	121	0.000
58	22 / 9	Inclusion within cordierite (SG)	2755	66	2754	122	0.000
59	22 / 10	Inclusion within cordierite (SG)	2795	67	2794	124	0.000

Table 1b. *(Continued.)*

Sl. no.	point	Mode of occurence	EXPLICIT AGE (Ma)	AGE error(1σ, Ma)	Age (Ma) Calculated from Montel equation	Age error (Ma,2σ) claculated by Vlach (2010) method	Y
60	23 / 1	Inclusion within garnet (SG)	2902	69	2900	128	0.000
61	23 / 2	Inclusion within garnet (SG)	3109	94	3107	136	0.041
62	23 / 3	Inclusion within garnet (SG)	2717	66	2716	123	0.000
63	24 / 1	Inclusion within cordierite	2738	65	2737	120	0.003
64	25 / 1	Inclusion within cordierite	2806	68	2805	124	0.009
65	26 / 1	Inclusion within cordierite	2651	63	2650	117	0.000
66	27 / 1	Inclusion within garnet	2858	71	2857	126	0.030
67	1 / 2	Inclusion within garnet	2903	67	2902	122	0.012
68	1 / 3	Inclusion within garnet	2864	65	2863	122	0.010
69	3/1	Inclusion within garnet	2752	66	2750	114	0.014
70	4/1	At the periphery of garnet (SG)	2904	68	2903	106	0.014
71	4/2	At the periphery of garnet (SG)	2813	65	2812	118	0.000
72	4/3	At the periphery of garnet (SG)	2783	65	2782	120	0.000
73	4/4	At the periphery of garnet ((SG))	2777	65	2776	118	0.000
74	4/5	At the periphery of garnet (SG)	2746	64	2745	118	0.000
75	5/1	At the periphery of garnet (SG)	2784	65	2783	123	0.000
76	6 / 1	At the periphery of garnet	2868	67	2866	120	0.000
77	7 / 1	At the periphery of garnet	2819	67	2818	137	0.001
78	9 / 1	At the periphery of garnet	2799	68	2798	88	0.000
79	10 / 2	At the periphery of garnet	3010	68	3009	138	0.001
80	10 / 3	At the periphery of garnet	2962	72	2960	114	0.001
81	10 / 4	At the periphery of garnet	3037	69	3036	103	0.002
82	10 / 5	At the periphery of garnet	3063	69	3062	108	0.003
83	11 / 1	Matrix (SG)	2826	70	2825	468	0.001
84	13 / 1	Inclusion within garnet (SG)	2912	102	2910	217	0.000
85	13 / 2	Inclusion within garnet (SG)	2950	89	2949	212	0.000
86	13 / 3	Inclusion within garnet (SG)	2871	109	2870	186	0.000
87	13 / 4	Inclusion within garnet (SG)	2707	90	2706	69	0.000
88	13 / 5	Inclusion within garnet (SG)	2694	64	2693	72	0.000
89	14 / 1	Inclusion within garnet (SG)	3069	70	3067	105	0.000
90	15 / 1	Inclusion within garnet (SG)	2930	67	2929	148	0.212

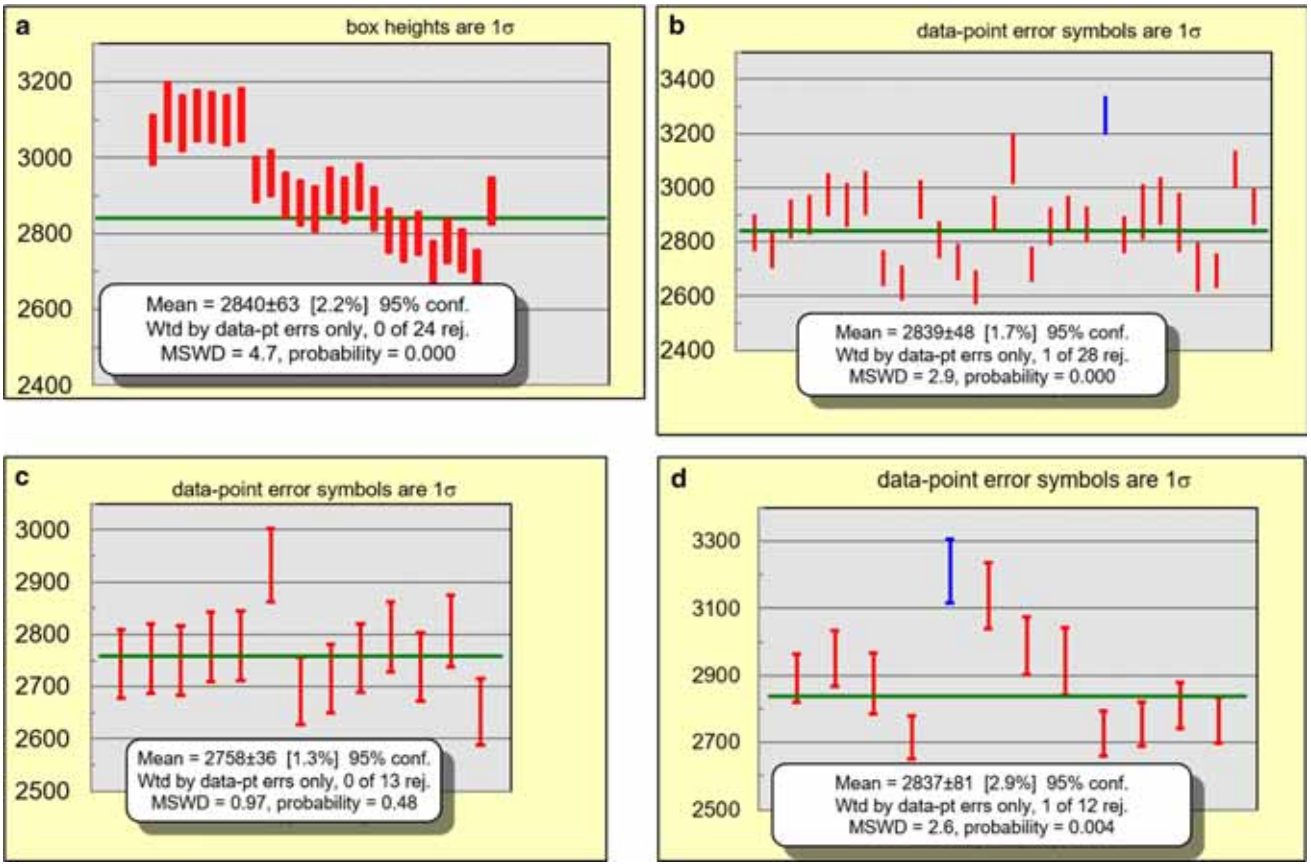

Figure 3. (**a–d**). Weighted average age (calculated using isoplot 4.15) of monazite occurring in matrix, as inclusion within garnet, cordierite and biotite respectively.

can be calculated by propagating the 1σ concentration error of Pb, U, Th through the age equation according to Bevington and Robinson (2003) method. But the elemental errors cannot be propagated through Montel *et al.* (1996) equation as it has no exact solution and can only be solved iteratively. Vlach (2010) devised a method for age and error calculation from EPMA analysis of monazite. Vlach (2010) reduced the $e^{\lambda t}$ term to $1 + \lambda t$ by applying first degree of Taylor–Mclaurin expansion of age equation devised by Montel *et al.* (1996) and developed the equation:

$$t = 22500 \times (Pb_T - Pb_0)/Th + 3.14 \times U. \quad (1)$$

Vlach (2010) calculated the age errors by propagating the uncertainties of U, Th and Pb through the 2nd degree Taylor–Mclaurin expansion of the age equation. However, this process has a dispute that precision of age error decreases with decreasing age (Sabau 2012). To overcome these difficulties in age and age error calculation, Sabau (2012) introduced explicit age and error calculation method. In this process, he started with classical decay equation ($dN/dt = -\lambda N$) and by reducing the term $e^{\lambda t}$ to $1 + \lambda t$ by applying first degree Taylor–Mclaurin expansion, subsequently proposed two equations for approximation of age for U and Th bearing phases respectively.

$$t1 = 138.88 \times Pb/10^6(137.88\lambda_{238} + \lambda_{235}) \times U \quad (2)$$

$$t1 = 10^{-6} \times Pb/\lambda_{232} \times Th + (137.88\lambda_{238} + \lambda_{235}) \times U/138.88 \quad (3)$$

Age errors were calculated according to Bevington and Robinson (2003) method by propagating the elemental uncertainties of U, Th and Pb through equation (3). For the present study, age was calculated both by iteratively solving the Montel *et al.* (1996) age equation and also with the explicit age equation. Age errors were calculated by both the method devised by Vlach (2010) and also by Sabau (2012). The ages of all the 90 monazite spot analysis from 27 grains

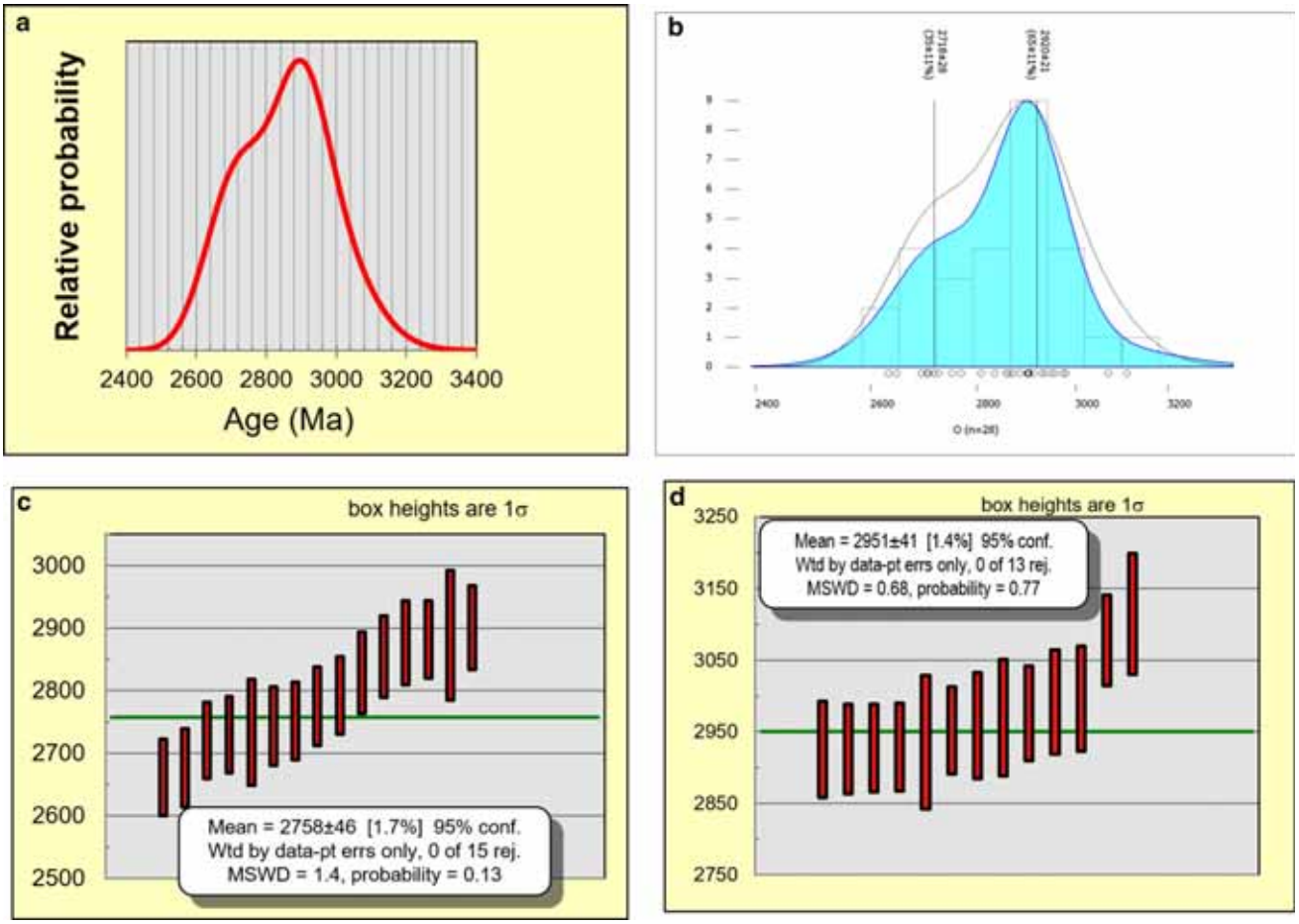

Figure 4. (**a**) Probability density plot (calculated using isoplot 4.15) of monazite inclusions in garnet shows a single prominent peak in between 2840 and 2960 Ma. (**b**) Kernel density estimate (KDE) plot of monazite inclusions in garnet shows a prominent peak in around 2920–2718 Ma. (**d, e**) Sub-grouped weighted average age (calculated using isoplot 4.15) of monazite occurring as inclusion within garnet.

are calculated by explicit age equation ranges from 2611 to 3211 Ma and calculated by Montel *et al.* (1996) equation ranges from 2610 to 3209 Ma (table 1b). The weighted average of all the ages calculated by Vlach (2010) method is 2837 ± 28(2σ) Ma (MSWD = 4.8) while the weighted average of the ages calculated by explicit method is 2833 ± 27(1σ) Ma (MSWD = 3.3). In this paper, age and age error calculated by explicit (Sabau 2012) method has been used henceforth for all the discussions. Monazite ages are pooled into separate groups according to their mode of occurrence. Monazite grains (occurring in matrix) yield a weighted average age of 2840 ± 63 Ma (MSWD = 4.7, probability = 0, figure 3a), inclusions within garnet yield a weighted average age of 2839 ± 48 Ma (MSWD = 2.9, probability = 0, figure 3b), Monazite grains occurring immediately outside the garnet boundary show a weighted average age of 2866 ± 72 Ma (MSWD = 2.9, probability = 0.001), inclusions within cordierite show weighted average age of 2758 ± 36 Ma (MSWD = 0.97, probability = 0.48, figure 3c), inclusions within biotite show a weighted average age of 2837 ± 81 Ma (MSWD = 2.4, probability = 0.004, figure 3d). Therefore, from the above data it can be seen that all the pooled ages of monazite (except monazite inclusions within cordierite) in different mode of occurrences are showing very high MSWD and very low probability. This suggests very high variability of ages within similar mode of occurrences. Sabau (2012) suggested that weighted averages can only be meaningful if MSWD is very low and probability of it is very high. Săbău and Negulescu (2013) advocated towards a *true bottom-up approach* considering individual analysis separately and age pooling

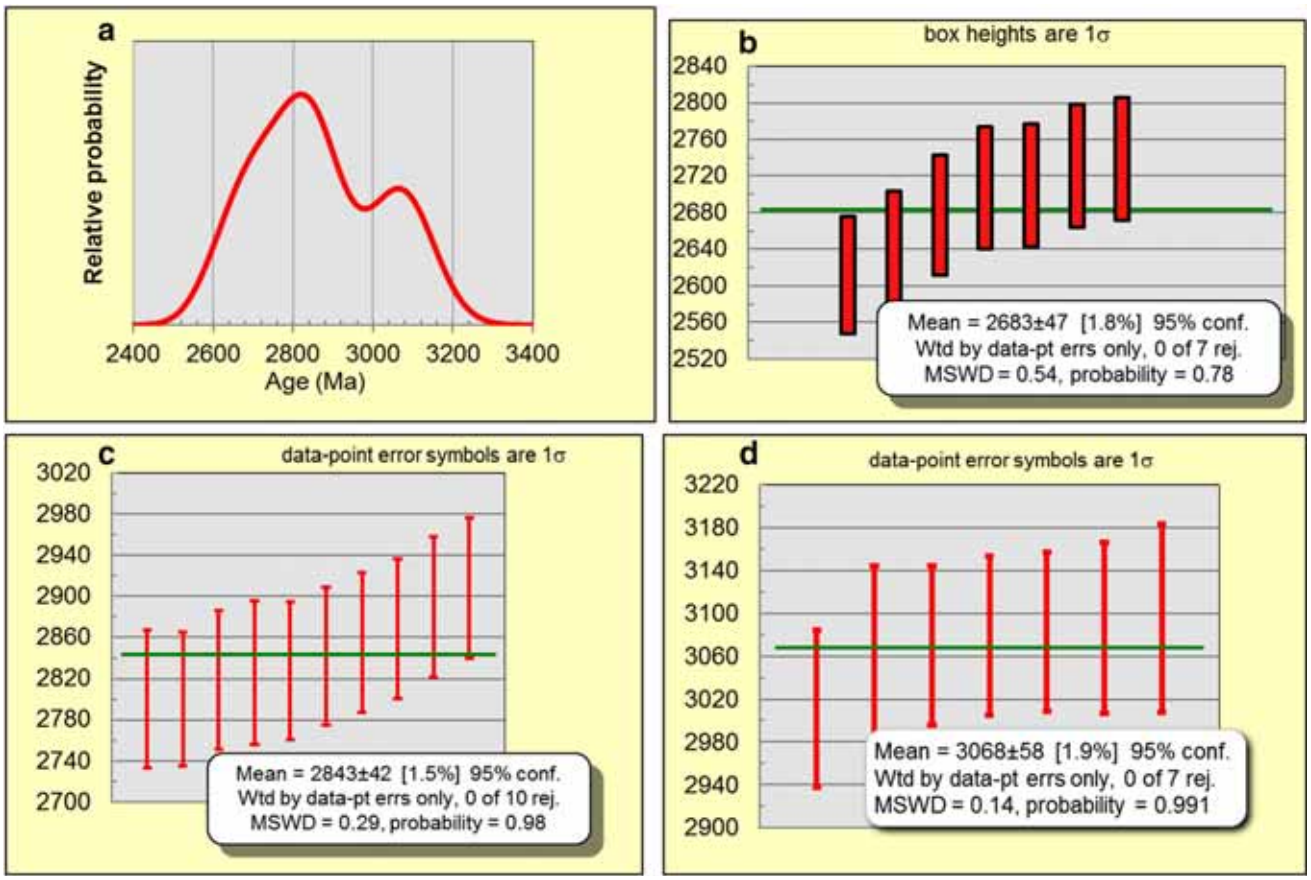

Figure 5. (**a**) Probability density plot (calculated using isoplot 4.15) of matrix monazite grains. (**b, c, d**) Sub-grouped weighted average age (calculated using isoplot 4.15) of matrix monazite.

based on different statistical methods. Generally, in a bottom-up approach, age data are pooled according to homogenous compositional domains in monazite. Sabau (2012) suggested several statistical methods for age pooling such as use of probability density function, age sorted plot and age gradient plots. Hence individual weighted average age for a particular mode of occurrence has again been divided into smaller sub-groups. For this purpose, several statistical plots (using isoplot-4.15) have been used such as probability density plot, linearized probability plot and age sorted plot. Probability density plot of monazite inclusions in garnet shows a single prominent peak between 2840 and 2960 Ma (figure 4a) with a slight rounded hump at 2720 Ma. Use of Kernel density plot (KDE) after Vermeesch (2012) also shows similar pattern as probability density plot and two distinct populations of ages, viz., one around 2920 Ma and another around 2718 Ma (figure 4b). Based on the plots, the monazite (inclusion within garnet) ages have been grouped into two sub-groups, viz., ages <2900 Ma and ages >2900 Ma showing weighted average age of 2758 ± 46 Ma (MSWD: 1.4, probability: 0.13, figure 4c), 2951 ± 41 Ma (MSWD = 0.68, probability = 0.77, figure 4d). Similarly, monazite grains occurring in matrix have also been subdivided in to sub-groups depending on probability density plot, which show two peaks, one sharp peak around 2800 Ma and another peak around 3000–3120 Ma (figure 5a). So matrix monazite ages have been divided into three sub-groups, viz., <2800, 2800–3000 and >3000 Ma showing weighted average age of 2683 ± 47 Ma (MSWD = 0.54, probability = 0.78), 2843 ± 42 Ma (MSWD = 0.29, probability = 98) and 3068 ± 58 Ma (MSWD = 0.14, probability = 0.99, figure 5b, c, d). Probability density plot of monazite inclusions within biotite show broad positive skewed nature with a peak around 2780 Ma (figure 6a). Hence the ages are clubbed together giving a mean weighted average age of 2897 ± 93 Ma (MSWD = 3.7, probability = 0, figure 6b). Monazite grains occurring immediately outside the garnet boundary show two peaks, one

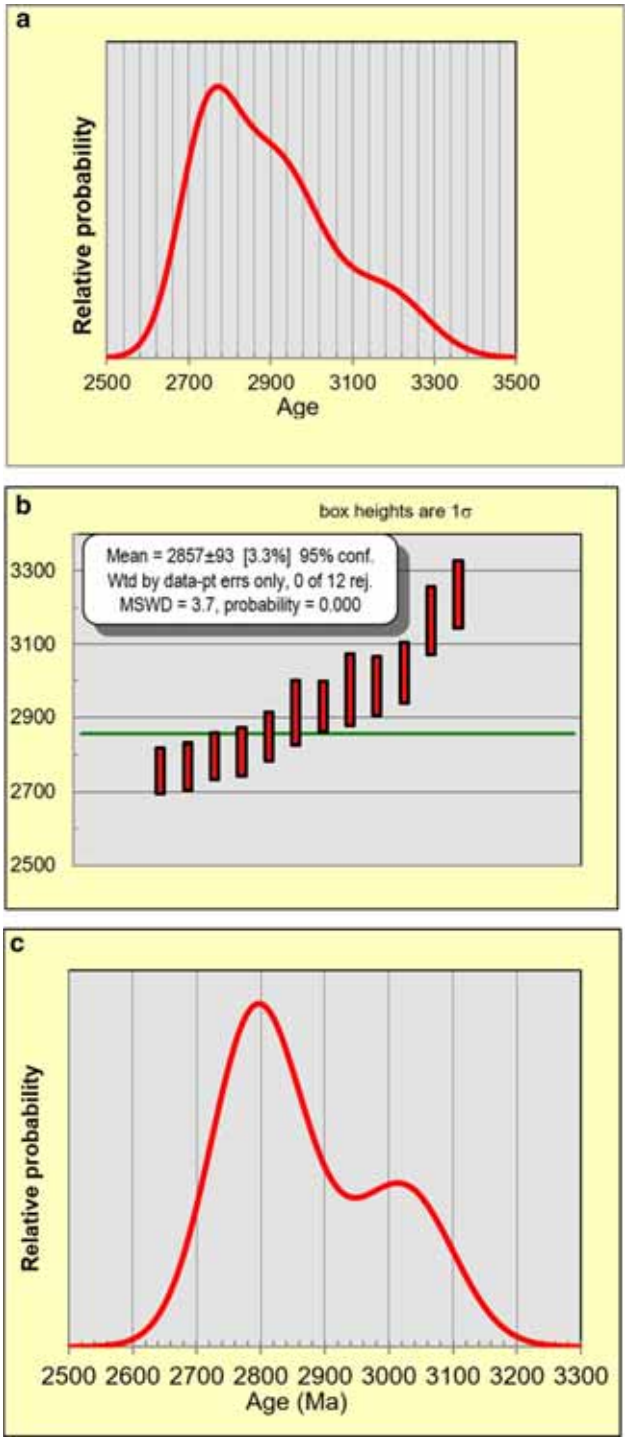

Figure 6. (**a**) Probability density plot (calculated using isoplot 4.15) of monazite inclusions in biotite shows a single prominent peak in between 2840 and 2960 Ma. (**b**) Weighted average age (calculated using isoplot 4.15) of all the monazite occurring as inclusion within biotite. **(c)** Probability density plot (calculated using isoplot 4.15) of monazite grains occurring just outside the margin of garnet.

sharp peak around 2800 Ma and another peak around 3000–3120 Ma similar to matrix monazites (figure 6c).

Probability density function plot for all the 90 monazite spot analysis from 27 grains shows slight positively skewed nature with a prominent peak near 2800Ma (figure 7a). Age sorted plot shows a nearly smooth line except little breaks near (marked with red circle) 2700 and 3000 Ma (figure 7b). Linearized probability plot of all the data also show similar pattern (figure 7c) with significant departure of points from the line around 2700 and 3000 Ma. Hence based on the above plots we have clubbed ages in to three groups, viz., <2700, 2700–3000 and >3000 Ma showing mean weighted average ages of 2654 ± 44 Ma (MSWD = 0.22, probability = 0.99), 2818 ± 19 Ma (MSWD = 1.3, probability = 0.044), and 3071 ± 41 Ma (MSWD = 0.36, probability = 0.98) respectively and isochron age (after Cocherie and Albarede (2001)) show mean weighted average age of 2743(+40–72) Ma, 2889(+36–35) Ma, 3076(+14–16) Ma (figure 7d, e, f).

Individual age traverses are taken along several monazite grains. Traverses along three monazite grains occurring as inclusions within garnet show a general trend of decreasing age towards the periphery (figure 8a, b). The cores of monazite inclusions within garnet show ages higher than 2900 Ma while the peripheral ages are much younger around 2700 Ma (figure 8a, b). Occurrence of monazite within garnet as an inclusion is very common in meta-pelites and is strongly controlled by occurrence of garnet as it is the host of REEs and Y. Content of Y in monazite is strongly correlated with garnet as monazites formed after the formation of garnet are low in Y in comparison to monazites formed earlier than garnet (Spear and Pyle 2010). In the present case the Y content of monazite grains varies widely according to their mode of occurrence. Monazite grains occurring as inclusion near the center of garnet show higher Y content than any other grains, while monazite inclusions within cordierite show no Y suggesting their growth later than garnet. However, monazite grains occurring just outside the margin of garnet or near the margin of the garnet (table 1a, point 4/1 to 4/5 and point 13/1 to 13/5) show negligible Y, probably due to their relatively late formation than those included in garnet. As discussed earlier this also corroborates with the two age populations of monazites in garnet, one around 2750 Ma another around 2950 Ma. Monazite grains occurring near the core of garnet are subhedral in nature (figure 8b), but monazite grains occurring near the margin of garnet (figure 8a) or just at the outer

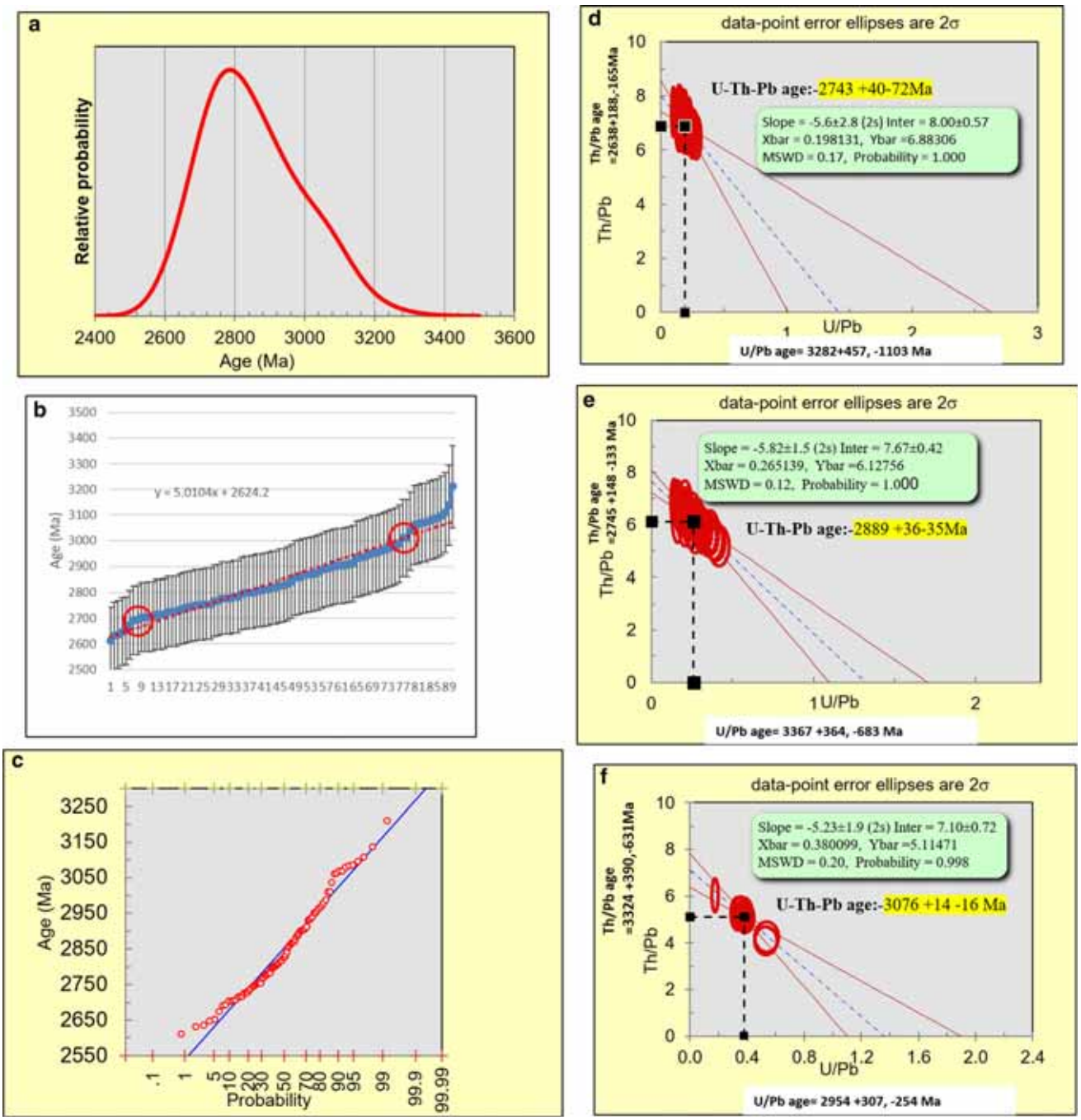

Figure 7. (**a**) Probability density function plot for all the 90 monazite spot analysis showing a slight positively skewed nature with a prominent peak near 2800 Ma. (**b**) Age sorted plot of all the 90 monazite spot analysis shows a nearly smooth line except little breaks near 2700, 2900 and 3060 Ma. (**c**) Linearized probability plot of all the 90 monazite spot analysis. (**d**, **e**, **f**). Isochron (after Cocherie and Albarede 2001) age of all the monazite analysis divided into three sub-groups, viz., <2700, 2700–3000 and >3000 Ma.

margin of the garnet are relatively anhedral in nature (figure 8c, d, e, f). Monazite grains occurring within matrix are of two types, the older grains (age around 3000 Ma) are anhedral while the younger grains (age around 2700 Ma) are subhedral (figure 9a, b, c, d). Older matrix monazites show higher amount of Y (point 7/1–7/6) than the younger ones (11/1, 12/1, 13/1–13/8) suggesting that the older matrix monazite grains formed before the garnet growth and younger ones after the garnet growth. It is considered that monazite grains occurring as inclusion within garnet or

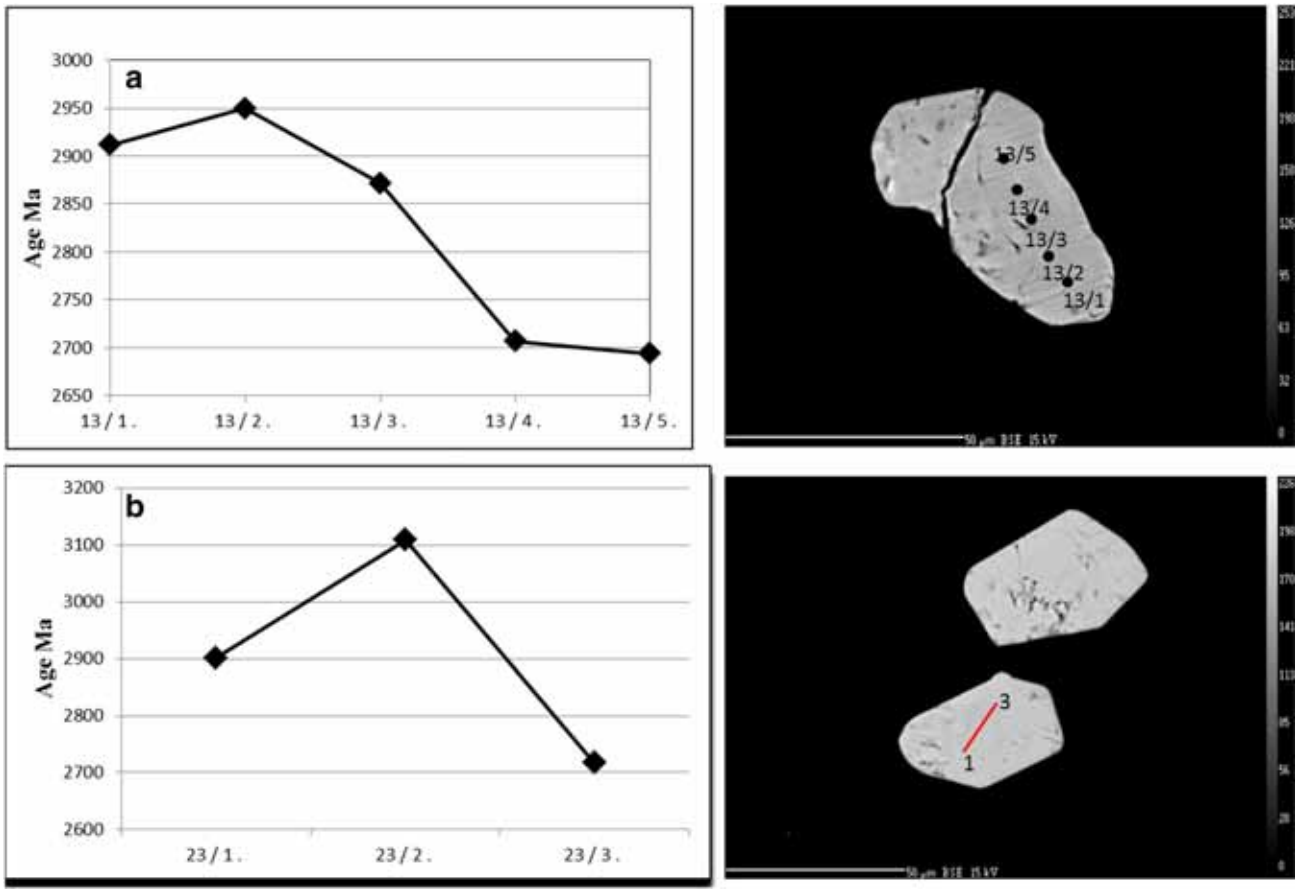

Figure 8. (**a**, **b**). Age traverses along monazite grains occurring as inclusions within garnet. (c). Monazite grain occurring near to the core of garnet. (**d**) zoomed image of figure (**b**), (**e**) monazite grain occurring just outside the margin of garnet, (**f**) zoomed view of figure (**e**).

cordierite are shielded from the metamorphic fluids (Catlos *et al.* 2002; Martin *et al.* 2007) and are generally immune to Pb loss. Pb content of matrix monazites are often re-equilibrated from interaction with metamorphic fluids and their preservation potential of older ages are often low than monazite included within garnet or any other porphyroblast (Catlos *et al.* 2002; Martin *et al.* 2007). But in present case, monazites included within garnet and cordierite are found to be younger than oldest of matrix monazites, suggesting lack of Pb re-equilibration. Monazite inclusion in cordierite shows euhedral shape (figure 9e, f) and nearly flat age pattern except a peak at the center (figure 9f). The euhedral shape of monazites also corroborate with their younger age. The wide variation of ages within a single grain indicates slow crystallization rate and episodic growth of the monazite grains (Catlos *et al.* 2002). Pb loss might be insignificant in this case as highest metamorphic temperature recorded is 673°C which is far below the closure temperature of 800°C. The younger subhedral matrix monazite grains may have formed by dissolution of small older matrix monazites during retrogradation (Catlos *et al.* 2002).

6. REE pattern of monazites

The source of REE for the monazites occurring in lower greenschist facies condition are probably the REE enriched clays or hydro-phosphates (Spear and Pyle 2002). Total six REE elements (La, Ce, Pr, Nd, Sm, Gd, Dy) were estimated for all the 90 monazite spot analysis (table 1a). Chondrite normalized REE pattern of individual grains are also plotted (in diagram) to assess the relation with corresponding age traverses. Chondrite normalized REE pattern of monazite inclusions within garnet shows that analysis points having <2800 Ma age are showing distinctly lower MREE values than older spots (figure 10a). In case of matrix

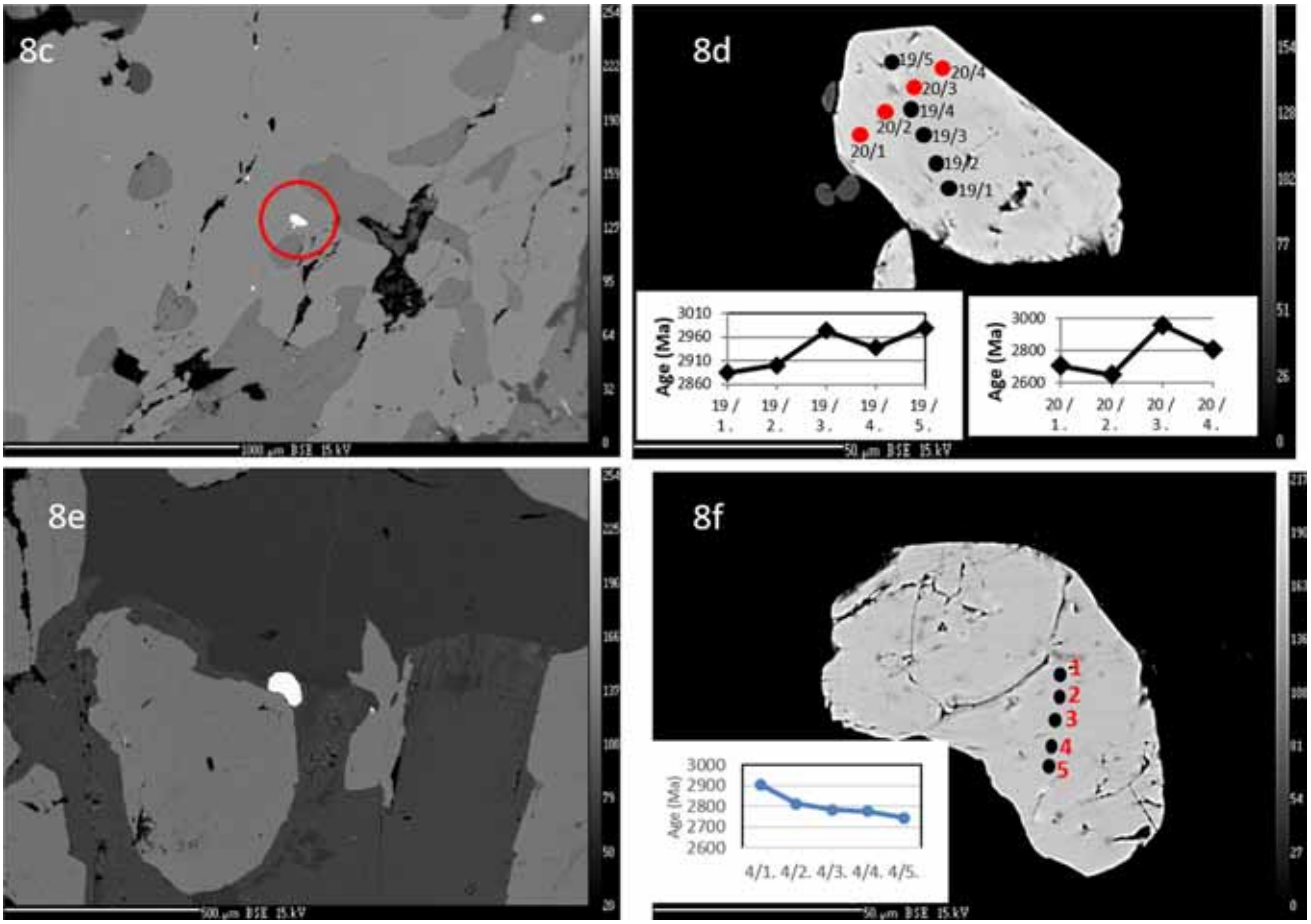

Figure 8. (*Continued.*)

monazites also similar pattern (figure 10b) is observed. REE pattern of monazite inclusion within cordierite show high MREE for only two points (point 22/6, 8/1) corroborating with its older age (figure 10c), while other points (of younger age) show distinctly lower MREE values. When all the spot analyses are clubbed together irrespective of their mode of occurrence, the REE pattern show wide range in MREE values (figure 10d) with considerable overlap between >3000 and 2800–3000 Ma spot ages but show distinctly lower MREE for <2800 Ma spot ages (table 2, figure 10d).

7. Discussion and conclusion

Santosh *et al.* (2003) have reported age data on zircon, monazite and uraninite recovered from granulite facies assemblages from KGB and BGB based on electron microprobe analyses (EPMA). Karimnagar granulite belt occurs around 100 km north of the Yerrabali Schist Belt. Bhopalpatnam granulite belt occurs to the east of Karimnagar Granulite belt (figure 1a). The Bhopalpatnam granulite belt, is about 300 km long and 20–40 km wide occuring along the SW margin of the Bastar craton. The main rock types are younger granite, two-pyroxene granulite, O1–Spl–Opx-bearing ultramafics, charnockite and charnockitic gneiss of tonalite-trondhjemitic affinity, enderbite, quartzite, calcsilicate, Al- and Mg–A1 pelite, BIF, and gneiss–migmatites, banded gneiss with metaigneous and metasedimentary restites (Santosh *et al.* 2003). Karimnagar granulite belt extends for about 150 km with an approximate width of 20 km. The most predominant rock is a coarse grained unfoliated charnockite, which encloses a wide variety of high-grade supracrustals. The dominant type of rocks in the enclaves include charnockite–enderbite gneiss, ultrabasic–basic granulite, amphibolite, calc-granulite, Sapphire, Opx and cordierite-bearing pelites and a variety of psammitic rocks (Santosh *et al.* 2003). Magmatic zircons from KGB charnockites show core ages of up to 3.1 Ga

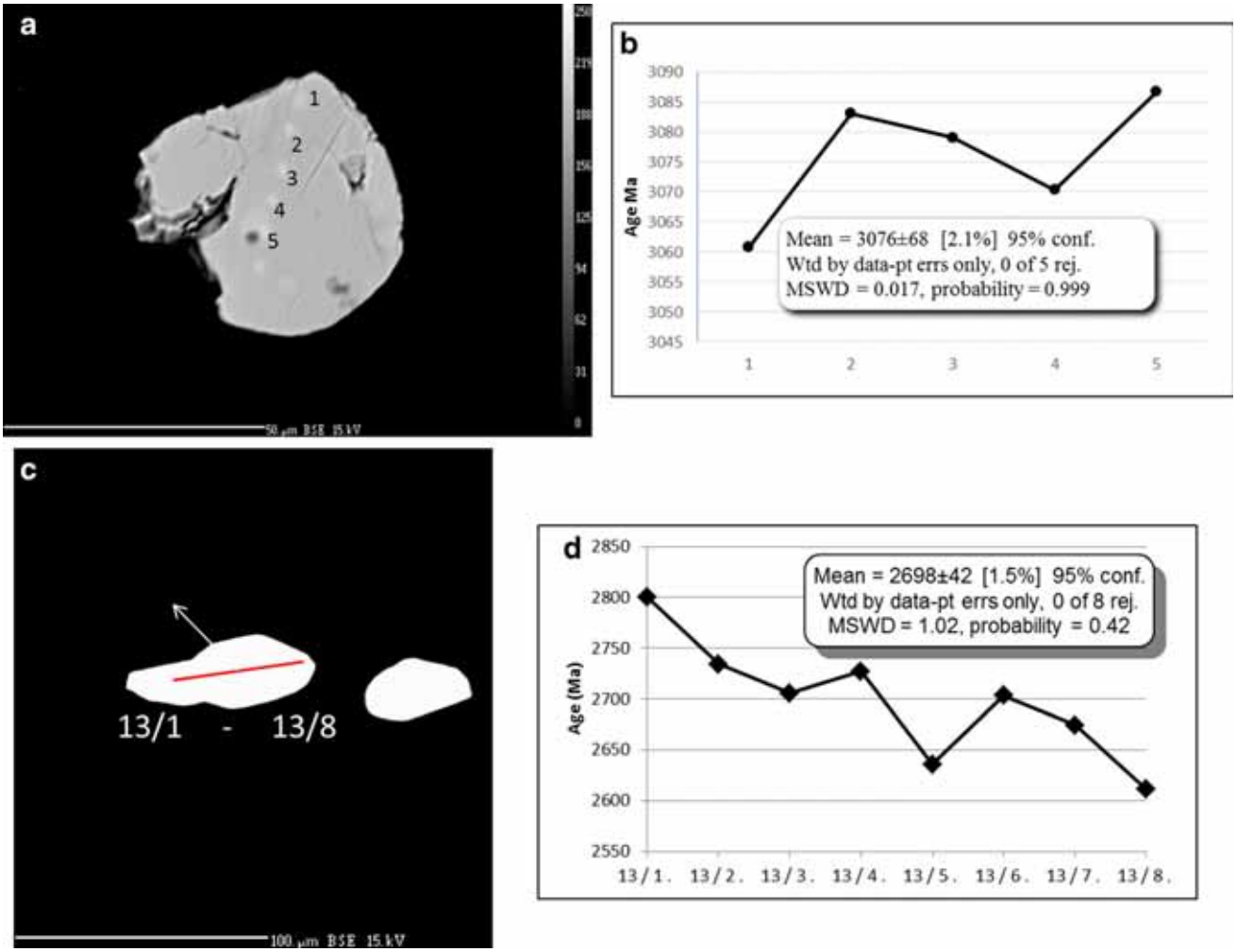

Figure 9. (a) Anhedral older matrix monazite grains. (**b**) Age traverse in older matrix monazite. (**c**) Subhedral younger matrix monazite grains. (**d**) Age traverse in younger matrix monazite. (e) Euhedral monazite occurring as an inclusion within cordierite. (**f**) Zoomed view of figure (**e**).

mantled by rims of 2.6 Ga showing a clear peak between 2.6 and 2.8 Ga registering mid to late Archean growth (Santosh *et al.* 2003). Zircons from BGB have 1.9 Ga cores mantled by 1.7 Ga rims. Monazites and uranitite from KGB show well-defined ages in the narrow range between 2.42 and 2.47 Ga, while monazites from BGB define a clear isochron age of 1.59 Ga (Santosh *et al.* 2003). The 1.7–1.6 Ga metamorphic age of BGB has been correlated with formation of Columbia supercontinent (Santosh *et al.* 2003). Santosh *et al.* (2003) suggested that KGB and BGB evolved under different pressure temperature conditions at different times, but recently Joy *et al.* (2018) reported 1600 Ma age of zircons from the southeastern part of KGB and have opined that both the belt was affected by same tectono-thermal event. Joy *et al.* (2018) have further reported 1000 Ma Grenvillian age from KGB. Grenvillian age is very prominent in Eastern Ghat Mobile belt (EGMB) and based on this, Joy *et al.* (2018) suggested that both EGMB and KGB were part of Grenvillian orogenic belt during Rodinia Supercontinent formation. Mukhopadhyay (2009), have provided a detailed tectono-metamorphic history of EGMB. Throughout EGMB, chemical dating of monazite has documented one major metamorphic event around 1 Ga, i.e., Grenvillian age and another much younger 500 Ma Pan-African event has been documented from the western part of EGMB. However, the imprint of Pan-African event has not been documented from the southern part (Ongole Domian) of EGMB (Mukhopadhyay 2009). Mahapatro *et al.* (2012) have documented evidences of archaean granulite metamorphism from the Rengali complex juxtaposed between EGMB and Singbhum craton

Figure 9. (*Continued.*)

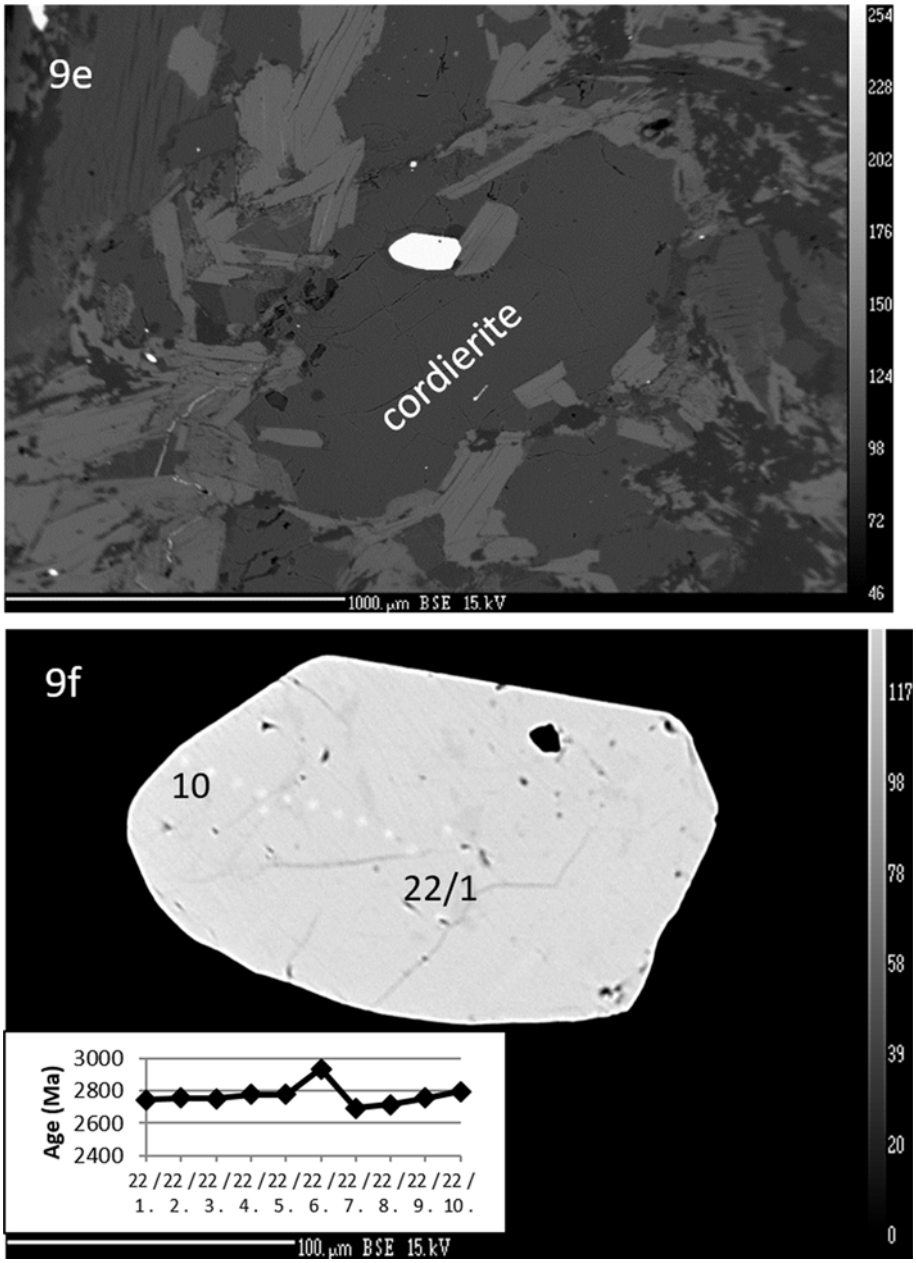

and have further advocated towards existence of oldest super continent Ur in that part and its extension up to 2.6 Ga.

EPMA ages of monazite grains obtained from the present study of the YSB do not match with the metamorphic monazite ages of KGB which are clustered around 2.4–2.47 Ga. This suggests that the metamorphic monazites of YSB are older than metamorphic monazites of KGB. Despite being older, the YSB shows middle to high amphibolite facies of metamorphism while KGB shows granulite grade of metamorphism. As described earlier, Singh and Dwivedi (2009) reported Garnet–cordierite–sillimanite–quartz assemblage from Bundelkhand craton and considered it to be indicative of granulite grade metamorphism. The lower temperature of YSB deduced from Fe–Mg exchange thermometers (garnet-biotite, garnet–cordierite) may be due to resettling of Fe, Mg of porphyroblasts due to slow cooling (Wu 2017; Mahapatro *et al.* 2012). Absence of muscovite from the present assemblage is an indication of high grade metamorphism. Muscovite decomposes to sillimanite and K-feldspar by the reaction Musc + qtz = K-feldspar + sillimanite at 4 kb pressure and 680°C temperature (Bucher and Frey 1994). However further work is required to bring out the

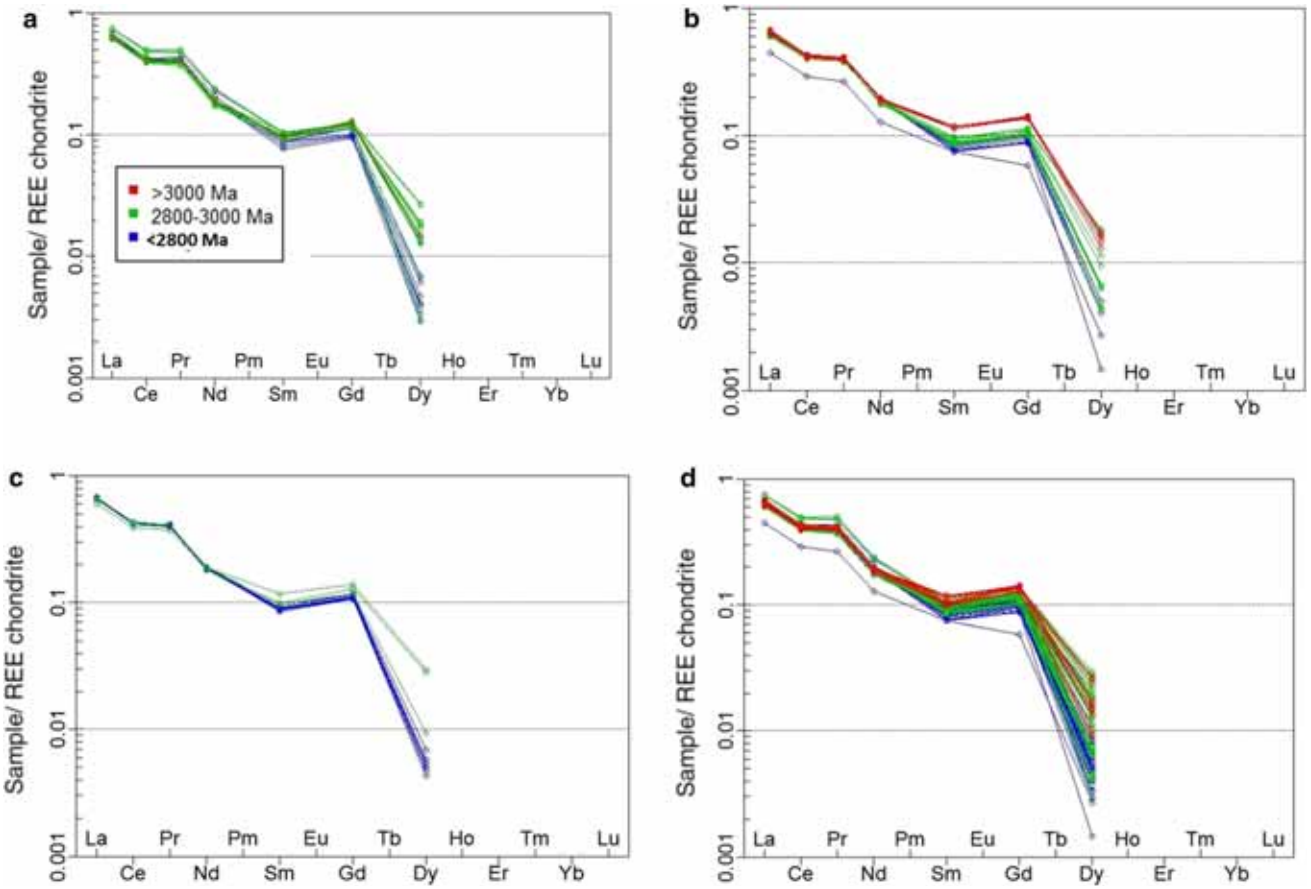

Figure 10. Chondrite normalised REE plot of **(a)** monazite grains occurring as incusion in garnet, **(b)** matrix monazite grains, **(c)** monazite occurring as incusion in cordierite, and **(d)** all 90 monazite spot analyses irrespective of their mode of occurence.

exact cause of difference of metamorphic grade between YSB and KGB.

Santosh *et al.* (2003) has opined that KGB which shows archaean protolith age is part of EDC while the younger mid-proterozoic BGB is a part of Bastar craton. Following the same line of logic YSB can also be considered as a part of EDC. This suggests that metamorphism in EDC started at mid-archaean time gaining peak around palaeo-proterozioc time (2.4 Ga) which is the dominant age of metamorphism of KGB. Prakash *et al.* (2017) have reported neoarchaen (∼2604 Ma) ages from the metamorphic zircons of High Mg–Al granulites near Jagtial area located at the north-eastern corner of EDC near KGB. From the above discussion it is evident that the metamorphism in Yerrabali schist belt started around 3000 Ma when oldest matrix monazite grains formed. In the present case, monazite is not preceded by allanite and hence may be assumed to have started forming in low-mid green schist facies condition, as the Ca content of the pelite controls the first appearance of monazite during metamorphism. Monazite is not thermodynamically stable during diagenesis of sediments (Spear and Pyle 2010). In Ca bearing meta-pelites, monazite appears at nearly 550°C by replacing allanite (Spear and Pyle 2010) and with increasing metamorphic grade size of monazite. In low Ca metapelites, monazites are reported to occur in chlorite–biotite zone in low-mid green-schist facies condition. Monazite grains included within garnet and cordierite grew around 2950 and 2758 Ma, respectively, probably constraining the occlusion age of garnet and cordierite suggesting cordierite growth later than garnet. From the above discussion it is evident that, metamorphism in YSB was episodic. The oldest episode occurred around 3000 Ma and continued in different phases up to 2700 Ma, thus constraining the protolith age of YSB to be of Palaeo–Mesoarchean. This suggests that YSB is older and not correlatable with Karimnagar granulite belt. However, further studies are required to work out the metamorphic evolution of YSB and to precisely constrain the age of different metamorphic phases.

Table 2. *EPMA analysis of garnet, biotite and cordierite.*

DataSet/Point	SiO2	TiO2	Al2O3	Cr2O3	FeO	MnO	MgO	CaO	NiO	Na2O	K2O	P2O5	F	Total
Garnet														
25 / 1	37.825	0.000	21.254	0.136	37.367	0.171	3.009	1.514	0.000	0.045	0.000	0.062	0.025	101.408
27 / 1	38.530	0.050	21.365	0.000	38.413	0.257	2.394	1.423	0.000	0.062	0.000	0.083	0.050	102.626
33 / 1	37.344	0.000	20.622	0.129	37.228	0.169	2.542	1.469	0.015	0.016	0.000	0.000	0.000	99.534
35 / 1	36.576	0.001	21.029	0.075	37.962	0.180	2.489	1.492	0.000	0.029	0.000	0.071	0.035	99.940
37 / 1	36.972	0.066	20.411	0.108	36.698	0.146	2.604	1.481	0.000	0.000	0.000	0.069	0.353	98.908
66 / 1	36.214	0.000	21.169	0.110	37.317	0.251	2.929	1.059	0.000	0.006	0.017	0.137	0.166	99.375
68 / 1	35.878	0.000	20.922	0.079	37.330	0.332	2.832	0.985	0.102	0.010	0.013	0.050	0.121	98.655
71 / 1	35.842	0.000	20.801	0.182	36.597	0.326	3.007	1.210	0.000	0.049	0.000	0.000	0.025	98.038
73 / 1	37.196	0.018	20.170	0.107	36.288	0.300	2.986	0.937	0.040	0.004	0.000	0.048	0.000	98.094
76 / 1	37.661	0.000	20.174	0.036	36.429	0.307	2.950	0.937	0.000	0.000	0.009	0.123	0.000	98.626
79 / 1	37.063	0.015	20.364	0.110	37.308	0.281	2.608	1.062	0.011	0.012	0.000	0.010	0.053	98.896
82 / 1	38.222	0.000	20.931	0.055	38.342	0.354	2.713	1.002	0.000	0.041	0.000	0.078	0.000	101.738
84 / 1	37.703	0.038	20.797	0.092	37.180	0.323	2.949	1.327	0.059	0.046	0.000	0.064	0.000	100.577
86 / 1	37.761	0.000	20.662	0.107	37.234	0.270	2.912	0.888	0.009	0.000	0.000	0.111	0.080	100.034
88 / 1	36.819	0.008	20.367	0.000	37.008	0.298	2.650	1.073	0.000	0.000	0.000	0.022	0.000	98.245

	Si	Ti	Al	Cr	Fe	Mn	Mg	Ca	Ni	Na	K	P
Recalculated cations on the basis of 24 oxygens												
p-25	6.870	0.000	2.287	0.010	5.676	0.026	0.815	0.295	0.000	0.016	0.000	0.005
p27	6.921	0.007	2.274	0.000	5.771	0.039	0.641	0.274	0.000	0.022	0.000	0.006
p-33	6.750	0.000	2.333	0.010	5.946	0.027	0.724	0.301	0.002	0.006	0.000	0.000
p-35	6.799	0.000	2.316	0.006	5.902	0.028	0.690	0.297	0.000	0.010	0.000	0.006
p-37	6.741	0.010	2.331	0.008	5.916	0.024	0.748	0.306	0.000	0.000	0.000	0.006
66/1	6.775	0.000	2.346	0.008	5.838	0.040	0.817	0.212	0.000	0.002	0.004	0.011
68/1	6.768	0.000	2.338	0.006	5.889	0.053	0.796	0.199	0.015	0.004	0.003	0.004
71/1	6.779	0.000	2.331	0.014	5.789	0.052	0.848	0.245	0.000	0.018	0.000	0.000
73/1	6.975	0.003	2.241	0.008	5.691	0.048	0.835	0.188	0.006	0.001	0.000	0.004
76/1	7.062	0.000	2.241	0.003	5.713	0.049	0.824	0.188	0.000	0.000	0.002	0.010
79/1	6.911	0.002	2.249	0.008	5.818	0.044	0.725	0.212	0.002	0.004	0.000	0.001
82/1	6.919	0.000	2.244	0.004	5.804	0.054	0.732	0.194	0.000	0.014	0.000	0.006
84/1	6.894	0.005	2.253	0.007	5.686	0.050	0.804	0.260	0.009	0.016	0.000	0.005
86/1	6.937	0.000	2.249	0.008	5.721	0.042	0.797	0.175	0.001	0.000	0.000	0.009
88/1	6.904	0.001	2.263	0.000	5.804	0.047	0.741	0.216	0.000	0.000	0.000	0.002

Table 2. *(Continued.)*

	Si	Ti	Al	Cr	Fe	Mn	Mg	Ca	Ni	Na	K	P		
Biotite														
Dataset/Point	SiO2	TiO2	Al2O3	Cr2O3	FeO	MnO	MgO	CaO	NiO	Na2O	K2O	P2O5	F	Total
28 / 1	35.482	3.106	18.783	0.255	21.296	0.013	7.688	0.082	0.027	0.367	9.373	0.000	0.105	96.575
30 / 1	34.174	2.984	18.469	0.209	21.161	0.000	7.700	0.083	0.094	0.261	9.334	0.056	0.145	94.670
32 / 1	35.638	3.625	18.263	0.287	21.843	0.000	7.457	0.042	0.143	0.184	9.600	0.000	0.225	97.308
34 / 1	35.249	3.484	19.196	0.302	19.752	0.000	7.927	0.082	0.118	0.173	9.702	0.000	0.250	96.237
67 / 1	33.515	2.321	18.087	0.274	20.147	0.060	8.621	0.066	0.148	0.904	8.764	0.052	0.102	93.062
77 / 1	34.473	2.159	18.543	0.238	20.341	0.000	8.659	0.045	0.070	0.341	8.777	0.000	0.375	94.020

	Si	Ti	Al	Cr	Fe	Mn	Mg	Ca	Ni	Na	K	P	X Mg	
Recalculated cations on the basis of 24 oxygens														
p-28	6.647	0.438	2.084	0.019	3.336	0.002	2.146	0.016	0.004	0.133	2.240	0.000	0.391	
p-30	6.567	0.431	2.102	0.016	3.401	0.000	2.205	0.017	0.015	0.097	2.288	0.005	0.393	
p-32	6.636	0.508	2.015	0.021	3.402	0.000	2.069	0.008	0.021	0.066	2.281	0.000	0.378	
p-34	6.621	0.492	2.136	0.023	3.103	0.000	2.219	0.017	0.018	0.063	2.325	0.000	0.417	
67/1	6.451	0.336	1.539	0.016	1.622	0.005	1.237	0.007	0.011	0.084	0.538	0.005	0.433	
77/1	6.636	0.313	1.578	0.014	1.637	0.000	1.242	0.005	0.005	0.032	0.539	0.000	0.431	
Cordierite														
DataSet/Point	SiO2	TiO2	Al2O3	Cr2O3	FeO	MnO	MgO	CaO	NiO	Na2O	K2O	P2O5	F	Total
75 / 1 .	48.535	0.000	31.961	0.000	9.156	0.000	7.362	0.030	0.000	0.163	0.020	0.000	0.028	97.255
78 / 1 .	49.685	0.000	31.074	0.000	8.576	0.003	7.477	0.014	0.087	0.185	0.000	0.000	0.000	97.101
80 / 1 .	49.077	0.003	32.293	0.000	8.982	0.000	7.687	0.018	0.015	0.207	0.000	0.000	0.103	98.385
83 / 1 .	49.939	0.000	31.007	0.000	9.563	0.000	7.069	0.016	0.000	0.260	0.020	0.007	0.117	97.998
85 / 1 .	49.035	0.010	31.956	0.000	9.085	0.027	7.653	0.008	0.009	0.172	0.010	0.000	0.000	97.965
87 / 1 .	49.924	0.000	31.421	0.010	9.268	0.000	7.153	0.000	0.022	0.201	0.000	0.037	0.082	98.118
Recalculated cations on the basis of 18 oxygens														
	Si	Ti	Al	Cr	Fe	Mn	Mg	Ca	Ni	Na	K	P	X Mg	
75/1	6.317	0.000	2.464	0.000	0.997	0.000	1.428	0.004	0.000	0.041	0.003	0.000	0.589	
78/1	6.467	0.000	2.396	0.000	0.933	0.000	1.450	0.002	0.009	0.047	0.000	0.000	0.608	
80/1	6.387	0.000	2.490	0.000	0.978	0.000	1.491	0.003	0.002	0.052	0.000	0.000	0.604	
83/1	6.500	0.000	2.391	0.000	1.041	0.000	1.371	0.002	0.000	0.066	0.003	0.000	0.568	
85/1	6.382	0.001	2.464	0.000	0.989	0.003	1.484	0.001	0.001	0.043	0.002	0.000	0.600	
87/1	6.498	0.000	2.423	0.001	1.009	0.000	1.387	0.000	0.002	0.051	0.000	0.002	0.579	

Acknowledgement

It is indeed a pleasing privilege for the authors to express their profound gratefulness to Shri P A Ramesh Babu, then-Deputy Director General, SU: AP, GSI, SR, Hyderabad, for his sustained interest, warm encouragement and valuable suggestions. The authors are indebted to EPMA Laboratory, GSI, CHQ, Kolkata, for providing high quality EPMA data. The authors acknowledge Dr. S Ravi (then-project director) for his insurmountable enthusiasm, expert supervision and excellent guidance.

References

Adhikary D, Sahoo R K, Behera K K and Krishna K V S S 2016 Zircon U–Pb dating of the TTG gneiss in and around Khammam area, Telangana, India – Evidence for the oldest crust in the Eastern Dharwar craton (EDC); 35th IGC abstracts.

Bevington R P and Robinson K D 2003 *Data reduction and error analysis for the physical sciences*; 3rd edn, United States, Mc. Graw Hill, Chapter 3.

Bucher K and Frey M 1994 *Petrogenesis of metamorphic rocks*; 6th edn, Heidelberg, Germany, Springer-Verlag.

Catlos E J, Gilley L D and Harrison M T 2002 Interpretation of monazite ages obtained via in situ analysis; *Chem. Geol.* **188** 193–215.

Chadwick B, Vasudev V N and Hedge G V 2000 The Dharwar craton, southern India, interpreted as the result of Late Archaean oblique convergence; *Precamb. Res.* **99** 91–111.

Cocherie A and Albarede F 2001 An improved U–Th–Pb age calculation for electron microprobe dating of monazite. *Geochim. Cosmochim. Acta* **65** 4509–4522.

Dwivedi S B, Mohan A and Lal R K 1998 Recalibration of the Fe–Mg exchange reaction between garnet and cordierite as a thermometer; *Eur. J. Mineral.* **10** 281–289.

Dwivedi S B, Mohan A and Lal R K 1997 Internally consistent geothermobarometers in the system FeO–MgO–Al_2O_3–SiO_2–H_2O involving garnet, cordierite, aluminosilicate and quartz and their application to metapelites; *J. Geol. Soc. India* **49** 647–660.

Fitzsimons I C W, Kinny P D, Wetherley S and Hollingsworth D A 2005 Bulk chemical control on metamorphic monazite growth in pelitic schists and implications for U–Pb age data; *J. Metamorph. Geol.* **23** 261–277.

Gupta R K and Nandhagopal N 2014 Report on preliminary exploration for iron ore around Yerrabali area, Karimnagar district, Andhra Pradesh; Unpublished report of GSI

Hoisch T D, Wells M L and Grove M 2008 Age trends in garnet hosted inclusions from upper amphibolite facies schist in the northern Grouse Creek Mountains, Utah; *Geochem. Cosmochim. Acta* **72** 5505–5520.

Holdaway M J 2000 Application of new experimental and garnet Margules data to the garnet–biotite geothermometer; *Am. Mineral.* **85** 881–892.

Jayananda M, Moyen J-F, Martin H, Peucat J-J, Auvray B and Mahabaleswar B 2000 Late Archaean (2550–2520 Ma) juvenile magmatism in the Eastern Dharwar craton, southern India: Constraints from geochronology, Nd-Sr isotopes and whole rock geochemistry; *Precambrian Res.* **99** 225–254.

Joy S, Linde G V D, Choudhury A K, Deb G K and Tappe S 2018 Reassembly of the Dharwar and Bastar cratons at ca. 1 Ga: Evidence from multiple tectonothermal events along the Karimnagar granulite belt and Khammam schist belt, southern India; *J. Earth Syst. Sci.* **127** 76.

Mahapatro S N, Pant N C, Bhowmik S K, Tripathy A K and Nanda J K 2012 Archaean granulite facies metamorphism at the Singhbhum craton-Eastern Ghats Mobile Belt interface: implication for the Ur supercontinent assembly; *Geol. J.* **47** 312–333

Maibam B, Goswami J N and Srinivasan R 2011 Pb–Pb zircon ages of Archaean metasediments and gneisses from the Dharwar craton, southern India: Implications for the antiquity of the eastern Dharwar craton; *J. Earth Syst. Sci.* **120** 643–661.

Maibam B, Gerdes A and Goswami J N 2016 U–Pb and Hf isotope records in detrital and magmatic zircon from eastern and western Dharwar craton, southern India: Evidence for coeval Archaean crustal evolution; *Precamb. Res.* **275** 496–512.

Martin A J, Gehrels G E and De Celles P G 2007 The tectonic significance of (U,Th)/Pb ages of monazite inclusions in garnet from the Himalaya of central Nepal; *Chem. Geol.* **244** 1–24.

Montel J M, Foret S, Veschambre M, Nicollet C and Provost A 1996 Electron microprobe dating of monazite; *Chem. Geol.* **131** 37–53.

Mukhopadhyay D 2009 The eastern ghats belt – a polycyclic granulite terrain; *J. Geol. Soc. India* **73** 489–518.

Nathan N P, Sundara R S, Natarajan V and Raman R 1995 Petrography and petrochemistry of the cordierite bearing metapelites of Nartamalai Area, Pudukkottai District, Tamil Nadu; *J. Geol. Soc. India* **46** 477–483.

Perera L R K 1984 Coexisting cordierite–almandine – A key to the metamorphic history of Sri Lanka; *Precamb. Res.* **25(4)** 349–364.

Prakash D, Chandra S P, Tewari S, Joshi M, Frimmel H E, Hokada T and Rakotonandrasana T 2017 Petrology, pseudosection modelling and U–Pb geochronology of silica-deficient Mg–Al granulites from the Jagtiyal section of Karimnagar granulite terrane, northeastern Dharwar craton, India; *Precamb. Res.* **299** 177–194.

Rajesham T and Nagarajan K 1990 Report on systematic geological mapping in parts of Karimnagar district, Andhra Pradesh; Unpublished report of GSI.

Săbău G and Negulescu E 2013 Microprobe U–Th–PbT dating of Monazite: Top down, bottom-up or au Rebours?; *Int. J. Geol. Sci.* **1** 20–29.

Săbău G 2012 Chemical U–Th–Pb geochronology: A precise explicit approximation of the age equation and associated errors; *Geochronometria* **39** 167–179.

Saha D and Deb P S 2013 Proterozoic evolution of Eastern Dharwar and Bastar cratons, India – an overview of the intracratonic basins, craton margins and mobile belts*; J. Asian Earth Sci.* **91** 230–251.

Santosh M, Yokoyama K and Acharyya S K 2003 Geochronology and tectonic evolution of Karimnagar and Bhopalpatnam Granulite Belts, Central India; *Gond. Res.* **7** 501–518.

Singh S P and Dwivedi S B 2009 Garnet–sillimanite–cordierite–quartz bearing assemblages from early archaean supracrustal rocks of Bundelkhand Massif, Central India; *Curr. Sci.* **97** 103–107.

Spear F and Pyle J 2002 Apatite, monazite, and xenotime in metamorphic rocks; In: Phosphates: Geochemical, geobiological, and materials importance (eds) Kohn M L, Rakovan J and Hughes J M, *Rev. Mineral. Geochem. Min. Soc. Am.*, pp. 293–335.

Spear F S and Pyle J M 2010 Theoretical modeling of monazite growth in a low-Ca metapelite; *Chem. Geol.* **273** 111–119.

Vlach S R F 2010 Th–U–Pb(T) Dating by electron probe microanalysis, Part I. Monazite: Analytical Procedures and Data Treatment; *Geol. USP Sér. Cient.* **10** 61–85.

Vermeesch P 2012 On the visualisation of detrital age distributions; *Chem. Geol.* **312** 190–194.

Williams M L and Jercinovic M 2002 Microprobe monazite geochronology: Putting absolute time into microstructural analysis; *J. Struct. Geol.* **24** 1013–1028.

Williams M L, Jercinovic M and Hetherington C J 2007 Microprobe monazite geochronology: Understanding geologic processes by integrating composition and chronology; *Ann. Rev. Earth Planet. Sci.* **35** 137–75.

Winter J D 2001 *An introduction to igneous and metamorphic petrology*, 1st edn., United States, Prentice Hall.

Wu C M 2017 Calibration of the garnet–biotite–Al_2SiO_5–quartz geobarometer for metapelites; *J. Metamorph. Geol.* **35** 983–998.

Corresponding editor: Saibal Gupta